Nanostructured Photodetectors: From Ultraviolet to Terahertz

*Hongyu Chen, Hui Liu, Zhiming Zhang, Kai Hu, and Xiaosheng Fang**

Inspired by nanoscience and nanoengineering, numerous nanostructured materials developed by multidisciplinary approaches exhibit excellent photoelectronic properties ranging from ultraviolet to terahertz frequencies. As a new class of building block, nanoscale elements in terms of quantum dots, nanowires, and nanolayers can be used for fabricating photodetectors with high performance. Moreover, in conjunction with traditional photodetectors, they exhibit appealing performance for practical applications including high density of integration, high sensitivity, fast response, and multifunction. Therefore, with the perspective of photodetectors constructed by diverse low-dimensional nanostructured materials, recent advances in nanoscale photodetectors are discussed here; meanwhile, challenges and promising future directions in this research field are proposed.

1. Introduction

During the past few decades, we have witnessed that the booming photoelectronic industry has transformed the world and stretched throughout every facet of our lives. As one of the most important optoelectronic devices, photodetectors, which possess the ability to transform light into electrical signals precisely, have been capturing intensive attention. Up to now, it has widely been shared that accurate detection of light from the ultraviolet (UV: 10–400 nm) –to the visible (vis: 400–760 nm) –to the infrared (IR: 760 nm to 1 mm) to the terahertz (THz: 0.1–10 THz) region is critical for a variety of industrial, medical, and environmental applications.[1] As shown in **Figure 1**, benefiting from the development of the semiconductor industry in leaps and bounds, photodetection systems working at different wavelength regions have played an important role in flame sensing, ozone sensing, convert communications,[2,3] air and water purification, environmental monitoring, video imaging, night vision,[4] materials identification,[5] early detection of small primary tumors,[6,7] and astronomical studies,[8,9] etc.

Photodetection systems consist mainly of photodetector and signal processing chips. Under the impetus of Moore's law, the feature size of highly integrated electronic devices has shrunk toward several nanometers. For instance, Intel has realized 22 nm technology.[11–13] More recently, Samsung announced mass production of a 14 nm mobile application processor, and IBM Research Alliance produced the industry's 7 nm node test chips.[14,15] Therefore, to realize a highly integrated photodetection system with high performance, it is essential to scale photodetectors down to the nanoscale for technological applications. Meanwhile, it is expected that further development of photodetectors will be faster and more efficient. However, conventional devices start to misbehave at the optical diffraction limit, when their size decreases to sub-wavelength scale. Subsequently, the photoelectric conversion efficiency of nanoscale photodetectors would be seriously impacted. To solve the contradictions in further development of nano-photodetectors with high performance, a reinforcement of techniques is urgently needed. Fortunately, as a new class of building blocks for fabricating photodetectors, nanostructured materials (at least one of three dimensions is in the 1–100 nm range) exhibit a huge potential to settle this convoluted issue due to their quantum-confinement effect, surface effect, nonlinear optical effect, and dielectric confinement effect.[16–18] For instance, thanks to the quantum-confinement and nonlinear optical effects of quantum dots (QDs) and photonic crystals, a desired bandgap could be created in gapless graphene. Moreover, nanoscale metallic and half-metallic materials exhibit fascinating optical properties, which can concentrate, route, and manipulate light at a sub-wavelength scale.[19–21] Therefore, inspired by these unique functional materials, a multitude of nanoscale photodetectors based on different novel materials and principles have been developed at a remarkable pace. To be specific, both traditional low-dimensional semiconductors and novel two-dimensional layered materials have been extensively studied, and much insight has been gained on tuning their optoelectronic properties by controlling their sizes and architectures. An increasing number of outstanding nanoscale photodetectors has been explored. Additionally, traditional photodetectors, in conjunction with different nanostructured materials, exhibit plenty of exciting functionalities, such as rewritable features,[22,23] and gas detection,[24–27] as well as optical logic gates,[28] etc. Therefore, the potential applications of nanostructured materials for fabricating photodetectors are truly impressive.

To lay solid ground for the practical applications of the aforementioned nanoscale photodetectors, exploring novel materials is crucial, with readily controlled size, shape, and composition, as well as application compatibility with present devices. Photodetectors focusing on several special topics, such as

Dr. H. Y. Chen, Dr. H. Liu, Z. M. Zhang, K. Hu, Prof. X. S. Fang
Department of Materials Science
Fudan University
Shanghai 200433, P. R. China
E-mail: xshfang@fudan.edu.cn

DOI: 10.1002/adma.201503534

two-dimensional layered materials, self-assembly thin films, plasmon-enhanced photoabsorption, and hybrid photodetectors, etc. are described in previous reviews.[29–33] To provide a comprehensive design guideline for a wide range of interdisciplinary researchers, this paper provides a current review of the state-of-the-art photodetectors based on both novel and traditional low-dimensional materials containing QDs, nanowires, two-dimensional layered materials, and nanofilms ranging from the UV to THz frequency region. Moreover, some intriguing technologies incorporated in this field are demonstrated in detail as well. Possible challenges and opportunities in the future development of these photodetectors are proposed in the last section.

2. Nanoscale Photodetectors Fabricated by Various Photoelectronic Materials

From the perspective of an engineer, fabricating photodetectors for practical applications is generally designed to satisfy the "5S" requirements: high sensitivity, high signal-to-noise ratio, high spectral selectivity, high speed, and high stability.[34,35] This means that quantum efficiency, response speed, and signal-to-noise ratio are the most important figures of merit used to characterize photodetectors. As a matter of fact, the ability to transform optical signals into electrical signals is determined by a complex process of electron–hole pair generation, transportation, and recombination within the photoelectronic materials. For instance, the response time of a photodetector is determined by three factors: the drift and diffusion time of photon-generated carriers, the lifetime of excess minority carriers, and the *RC* time constant (*R*: load resistance, *C*: capacitance) of the device.[36] In light of the above investigation, the performance of a photodetector is mainly dependent on the inherent characteristics of the photodetector's active materials. Therefore, to select materials more reasonable for fabricating photodetectors with higher performance, the fundamental physical properties of important photoelectronic materials are summarized in **Table 1**, and corresponding low-dimensional photodetectors are discussed in following sections. It is noteworthy that some photodetectors can be classified into more than one type (wavelength, materials, dimensions, etc.). As an example, graphene or QD-based photodetectors can be operated throughout multiband in the range of the UV–THz

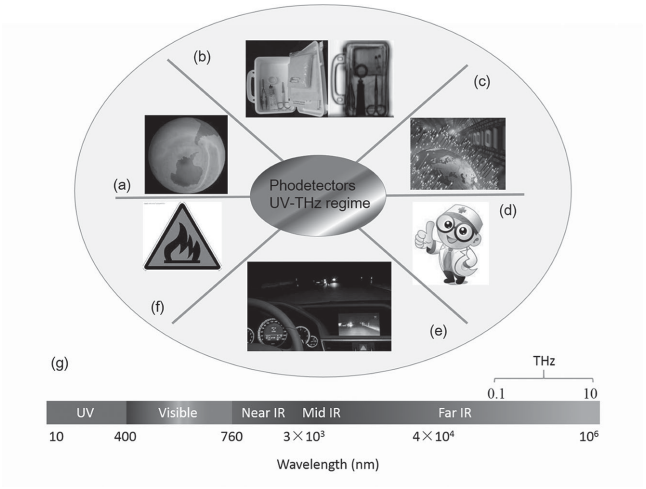

Figure 1. Versatile applications of photodetectors at the present or in the near future: a) ozone sensing, b) THz imaging, c) visible-light communication, d) detection of clinical medicine, e) infrared night-vision scope, f) flame detection, g) electromagnetic spectrum ranging from the UV to the THz regime. b) Reproduced with permission.[10] Copyright 2010, IEEE.

Hongyu Chen received her Ph.D. from State Key Laboratory of Luminescence and Applications, Changchun Institute of Optics, Fine Mechanics and Physics, Chinese Academy of Sciences in 2014. She is currently a postdoctoral fellow in the Department of Materials Science, Fudan University. Her current research interests include design, fabrication, and exploring novel properties of optoelectronic devices based on semiconductor and metallic materials, with a special focus on low-dimensional photodetectors.

Hui Liu received his Ph.D. from Fudan University in 2015 under the supervision of Professor Xiaosheng Fang. After that, he joined the Hubei Institute for Nationalities as a lecturer. His current research interests include synthesis, and optoelectronic and electrochemical applications of metal and semiconductor nanostructures, especially semiconductors based on niobium-related compounds.

Xiaosheng Fang is currently professor in the Department of Materials Science, Fudan University, China. After completing his Ph.D. degree at the Institute of Solid State Physics, the Chinese Academy of Sciences in 2006, he worked at the National Institute for Materials Science (NIMS), Japan as a JSPS postdoctoral fellow, and also as an International Center for Young Scientists (ICYS)–International Center for Materials Nanoarchitectonics (MANA) researcher. His research focuses on inorganic semiconductor nanostructure-based photodetectors.

Table 1. Basic parameters of semiconductors used in photodetectors ranging from UV to THz regime.

Band	Materials	p/n type (unintentionally doped)	E_g [eV]	Mobility [$cm^2 V^{-1} s^{-1}$]	Crystal structure	Lattice Constant [nm]	Indirect/ Direct	Carrier concentration [cm^{-3}]	Ref.
UV	AlN	n	6.2	2 (e)	Wurtzite	$a = 0.3112$ $c = 0.4982$	Direct	–	[32,43]
	Diamond	p	5.47	1800 (e) 1200 (h)	Cubic	0.357	Indirect	10^{15}	[32,36,44]
	β-Ga_2O_3	n	4.9	80–100 (e)	Monoclinic	$a = 1.223$ $b = 0.299$ $c = 0.577$	Direct	10^{17}–10^{18}	[45,46]
	ZnS	n	3.66	600 (e)	Zinc blende	0.541	Direct	–	[32]
	SnO_2	n	3.6	30 (e)	Rutile	$a = 0.478$ $c = 0.318$	Direct	10^{19}–10^{20}	[46,47]
	GaN	n	3.39	400 (e) 10 (h)	Wurtzite	$a = 0.3189$ $c = 0.5185$	Direct	10^{18}	[32]
	ZnO	n	3.37	200 (e) 180 (h)	Hexagonal	$a = 0.325$ $c = 0.5207$	Direct	10^{16}–10^{19}	[44]
	4H-SiC	n	3.26	1140 (e) 50 (h)	Hexagonal system	$a = 0.3081$ $c = 1.0061$	Indirect	10^{16}–10^{18}	[44,48]
	TiO_2	n	3.2	>10 (e)	Anatase	$a = 0.373$ $c = 0.296$	Direct	10^{21}	[49]
Visible	ZnSe	n	2.7	ca.400 (e)	Wurtzite	$a = 0.397$, $c = 0.652$	Direct	6.9×10^{16}	[50,51]
	CdS	n	2.5	350 (e) 40 (h)	Wurtzite	$a = 0.4136$, $c = 0.6714$	Direct	–	[36,52]
	V_2O_5	n	2.2	–	Orthorhombic	$a = 1.154$, $b = 0.3571$, $c = 0.4383$	Direct	–	[53]
	Cu_2O	p	2.1	62 (h)	Cubic	0.4266	Direct	–	[54,55]
	$NiCo_2O_4$	–	2.1	–	Cubic	0.974	–	–	[56]
Visible/ IR	WS_2	–	2.1 (monolayer)	–	Hexagonal	$a = 0.3154$ $c = 1.2362$	Direct (monolayer)	–	[57]
			1.4 (bulk)		Rhombohedral	$a = 0.3149$ $c = 1.8434$	Indirect (bulk)		
	Black Phosphorus	p	ca. 2 (monolayer) ca. 0.3(5) (bulk)	ca. 10 000–50 000 (e)	Rhombohedral	$a = 0.3138$ $b = 1.0477$ $c = 0.4376$	Direct		[58–61]
	MoS_2	n	1.8 (monolayer) 1.2 (bulk)	ca. 217 (e)	Hexagonal	$a = 0.3161$ $c = 1.2295$	Direct (monolayer) Indirect (bulk)	–	[62,63]
Visible	CdSe	n	1.74	500 (e)	Zinc blende	0.6050	Direct	3×10^{16}	[36,64]
	GaTe	p	1.7	0.2 (h)	Monoclinic	$a = 2.364$ $b = 0.4077$ $c = 1.046$	Direct	–	[65]
IR	InP	n	ca. 1.35	≤5400 (e)	Zinc blende	0.5869	Direct	$3 \times 10^{15} - 2.5 \times 10^{18}$	[66–68]
	Cd_3P_2	p	0.55	2.94 (h)	–	–	Direct	–	[69]
	Cd_3P_2	n	0.5	3000 (e)	–	–	–	10^{17}–10^{18}	[70]
	PbS	n	0.41	500–2000 (e)	Cubic	0.594	Direct	10^{16}–10^{18}	[71,72]
	PbTe	p	0.32	500–2000 (h)	Cubic	0.6454	Direct	10^{16}–10^{19}	[73–78]
	PbSe	n	0.29	500–2000 (e)	Cubic	0.613	Direct	10^{16}–10^{18}	[79–82]

regime.[37–39] Moreover, to realize higher performance of the devices, many different photodetectors have been constructed from different materials.[40–42] Therefore, to cover the breadth of nanostructured photodetectors available at the present time with suitable classification, avenues appear in this paper in the next sections in terms of the dimension (two-dimensions, one-dimension, and zero-dimension) of the device rather than the materials (III–V group or II–VI group semiconductors, semimetallic graphene, semiconducting transition-metal dichalcogenides) or operating wavelength (UV, visible, IR, and THz regime).

2.1. 2D Nanostructured Photodetectors

With one spatial dimension confined within the nanoscale, two dimensional (2D) materials especially in terms of 2D layered materials and solution-processed nanofilms exhibit many unique favorable properties for photodetection, which has stimulated extensive research over the past few years. Compared with the growth of conventional semiconductor films via universal epitaxial techniques, the above-mentioned 2D materials are usually fabricated by simpler methods, and most importantly, at lower cost. Moreover, with the flexible, transparent, high crystal quality features and rich physical properties, they have played an important role in constructing photoelectronic functional building blocks. Moreover, integrated with traditional technology, these versatile elements can demonstrate tremendous potential applications in fabricating new types of photodetectors with high performance. Therefore, recent research on photodetectors based on the previously mentioned 2D materials will be discussed in detail in the following sections.

2.1.1. Photodetectors Based on 2D Layered Materials

Since the discovery of graphene, as intriguing building blocks and new platforms in optoelectronic devices,[33,59,83–87] 2D layered materials have attracted a great deal of attention among researchers. Thanks to the extended family of 2D layered materials including semi-metallic graphene, semiconducting transition metal dichalcogenides (TMDCs) and the recently discovered few-layered black phosphorus (donated as "phosphorene"), and the insulating boron nitride, a wide selection of light detection spanning from the UV, visible, and infrared to the THz regime has been achieved.[59] Compared with conventional epitaxial membranes, they share quite a few advantages in constructing photodetectors. For instance, owing to their unique layered structures, atomically sharp 2D heterostructures can be realized without consideration of the lattice mismatches between different materials. Hence, in addition to functioning solely as photodetectors with high performance, it is easier for these 2D layered materials to combine each other's advantages by forming heterostructures through van der Waals interactions. Moreover, the ultra-thin feature of 2D layered heterostructures also allows for vertical modulation of the band structure, which opens an additional avenue for exploring 2D electronic and optoelectronic devices.[58,59] Therefore, photodetectors with high performance, such as broadband, ultra-fast, and ultra-sensitive, as well as multiple functions like flexibility, and transparency, and being self-powered, rewritable, and memonic, can be realized based on these layered materials. Herein, we will highlight recent progress with respect to photodetectors based on 2D layered materials in terms of graphene-based photodetectors, TMDC devices, and newly developed phosphorene-based photodetectors in the order of the history of their development.

Despite being only one single atomic layer thick, graphene is found to absorb a fraction of incident light as high as 2.3% owing to the 2D nature and gapless electronic spectrum.[88–90] Therefore, it is expected that photodetectors based on graphene should be able to detect light over a wide energy spectrum (from the UV to THz regime) based on the photoelectric/photovoltaic effects or on the photo-thermoelectric effect, which is unmatched by other materials.[91,92] In spite of these advantages, the performance of graphene-based photodetectors, especially with regard to responsivity, is still lower than expected. Fortunately, significant efforts, such as using hydrogenated graphene (to prolong the carrier lifetime and increase the internal quantum efficiency),[93] suspended graphene monolayers (to decrease the substrate scattering and enhance heat-conduction),[94,95] nanoribbons or nanomesh-structured graphene (to create a bandgap),[96] have been devoted to developing a broadband and high responsivity of photodetectors based on graphene.

In 2009, Xia et al. proposed that single or few-layer graphene can be used as ultra-fast photodetectors,[97] The photoresponse does not degrade for optical-intensity modulations up to 40 GHz, and the intrinsic bandwidth can be further improved by optimizing the structure of the device. Consequently, this leads to a remarkable interest in graphene photodetectors for ultra-fast, broadband functions. In 2014, Liu et al. realized an ultra-broadband photoresponse at room temperature by a double-layer graphene asymmetric tunneling barrier.[98] As shown in **Figure 2**a, the device is a phototransistor consisting of a pair of stacked graphene monolayers (top layer, bottom layer) separated by a thin tunnel barrier (gate, channel-Ta_2O_5, or silicon). In this architecture, the graphene functions not only as the light absorber but also as the charge-transport channel. It can be found in their energy band diagram in the inset of Figure 2b, benefiting from the top graphene layer that is more heavily p-doped relative to the bottom graphene layer, that the energy band of the tunneling barrier is tilted toward the bottom graphene layer in order to equilibrate the Fermi level. Taking advantage of this asymmetric tunneling barrier, a multitude of hot electrons could tunnel easily from the top to the bottom graphene layer. Specifically, when light is incident on the surface, photoinduced hot carriers will tunnel into the nearby graphene layer, leading to a charge build-up on the gate and a strong photogating effect on the channel conductance. Figure 2b displays the transfer curves for the bottom graphene layer under different silicon backgate voltages (V_{gb}) and optical powers. The transfer curve shifts dramatically toward negative V_{gb} with increasing laser power, which indicates that the efficient tunneling of high-energy hot electrons leads to a positive charge build-up in the top graphene layer, giving rise to a strong photogating effect and n-doping of the bottom graphene channel. The gate-modulated characteristics of the transfer curve offer convenient on–off switching control for photodetection. The

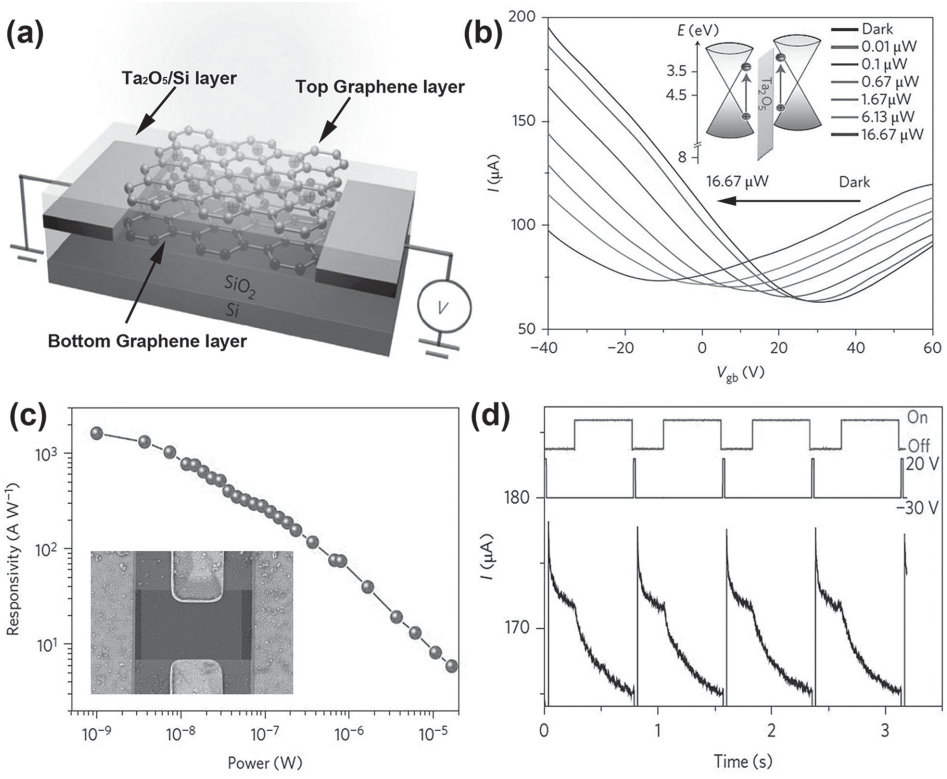

Figure 2. Sandwich-structured graphene photodetectors with ultra-broadband and high responsivity at room temperature. a) Schematic of the phototransistor. b) I–V_{gb} (silicon backgate) characteristics of the measured graphene photodetector under different laser powers. The potential of the top graphene layer was allowed to float, while the current of the bottom graphene transistor was measured under 1 V source–drain bias voltage. Inset: energy-band diagram of the graphene/Ta_2O_5/graphene heterostructures. c) Measured photoresponsivity versus illumination power. Inset: false-color scanning electron microscopy (SEM) image of the device. d) The time-dependent photocurrent measurement of the graphene photodetector (black curve). The illumination power is 0.3 μW and the laser wavelength is 532 nm. The laser on–off (red curve) is controlled by a mechanical shutter synchronized with the reset backgate pulses (blue curve). Reproduced with permission.[98] Copyright 2013, Nature Publishing Group.

calculated responsivity shows a strong dependence on the power of the incident light (Figure 2c). Under low excitation power (532 nm, ca. 10^{-9} W, continuous-wave semiconductor diode laser), the device shows a remarkable responsivity of 1000 A W^{-1} at a 1 V source–drain bias voltage, suggesting that a built-in amplification mechanism can efficiently convert the photon energy into a large electrical signal. Further to that, the temporal photoresponse under on–off light modulation with a 1 V bias voltage at room temperature (Figure 2d) also indicates that the present device possesses a fast photoresponse, and can be modulated by changing the backgate voltage pulses. Apart from the visible response, a high photoresponsivity in the near-infrared and mid-infrared regimes can also be achieved by incorporating intrinsic silicon as the tunnel barrier instead of the wide-bandgap Ta_2O_5 layer (Figure 2a). The near-infrared responsivity of a graphene/silicon/graphene device reaches 4 A W^{-1} at a wavelength of 1.3 μm and 1.1 A W^{-1} at a wavelength of 3.2 μm at room temperature, rivaling state-of-the-art mid-infrared detectors without the need for cryogenic cooling.

Great improvement in the responsivity has been realized for photodetectors based on graphene; however, there is an intractable issue for graphene-based devices: the high dark current arising from its gapless nature, which has a strong impact on the sensitivity of photodetection.[59,63] Alternatively, another kind of layered material, TMDCs with a natural gap, has captured much more attention in recent years. Up to now, TMDCs including MoS_2,[63,99,100] WS_2,[57,101] WSe_2,[102] InSe,[103] GaS,[104] GaTe,[65] GaSe,[105] and In_2Se_3,[106] have been explored to develop plenty of new photodetectors with favorable photoelectronic properties. To illustrate this kind of photodetector vividly, MoS_2-based photodetectors are taken as an example.

As a typical TMDC material, MoS_2 is composed of a vertical stack in which the weakly interacting layers are held together by van der Waals forces. It is noteworthy that bulk-form MoS_2 is a semiconductor with an indirect bandgap of 1.2 eV, whereas single-layer MoS_2 is another kind of semiconductor with a direct bandgap of 1.8 eV.[62] This unique property of MoS_2 stems from the effect of quantum confinement on its electronic structure.[107]

Figure 3a shows a schematic view of a single-layer MoS_2 photodetector, proposed by Lopez-Sanchez et al.[108] It is worth noting that the photoresponsivity of this device reaches 880 A W^{-1} at a wavelength of 561 nm, a bias voltage of V_{ds} = 8 V, and V_{gate} = –70 V, under a very low illumination intensity. The calculated noise-equivalent power (NEP) is about 1.8×10^{-15} W $Hz^{-1/2}$ (Figure 3b), which is even lower than that of commercial state-of-the-art silicon avalanche photodiodes based on p–n junctions (3×10^{-14} W $Hz^{-1/2}$). The spectral

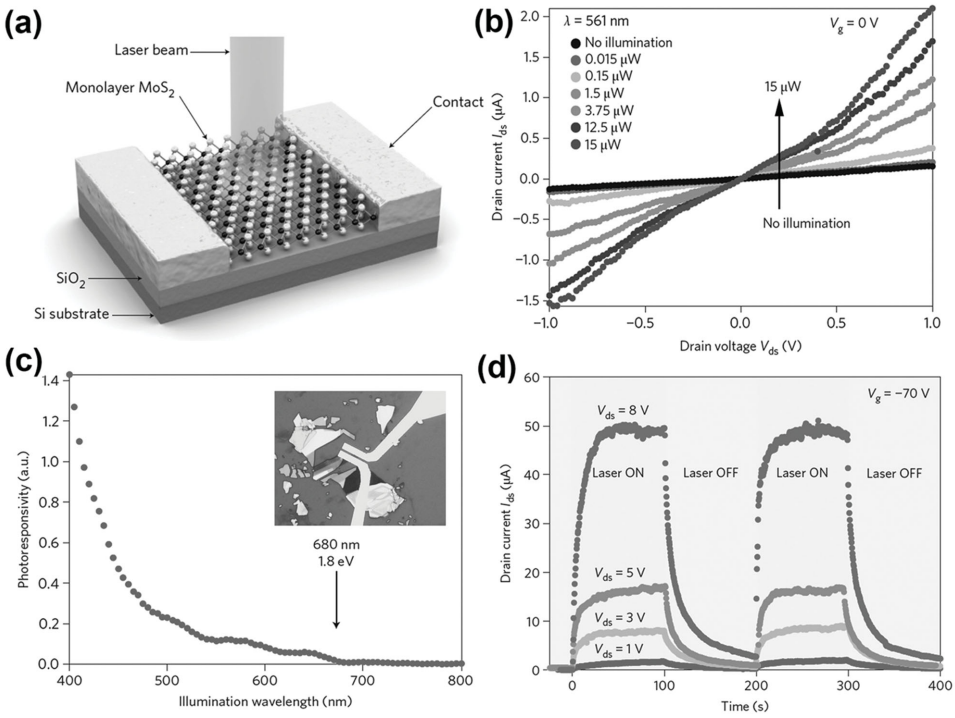

Figure 3. Ultra-sensitive photodetectors based on monolayer MoS_2. a) Three-dimensional schematic view of the single-layer MoS_2 photodetector and the focused laser beam used to probe the device. b) Drain–source (I_{ds}–V_{ds}) characteristics of the device in the dark and under different illumination intensities. The device operates as an enhancement-mode transistor. Increasing illumination levels result in enhanced current due to electron–hole pair generation by light absorption in the direct bandgap of monolayer MoS_2. c) Photoresponsivity versus illumination wavelength. d) Temporal photoresponse of the device under different values of bias voltage (V_{ds}), when the backgate voltage is –70 V and incident power is 0.425 μW. Reproduced with permission.[108] Copyright 2013, Nature Publishing Group.

response in Figure 3c indicates that the photoresponse range of the present device is 400–680 nm, which is consistent with the bandgap energy of monolayer MoS_2 (1.8 eV, corresponding to the energy of photons with a wavelength of 680 nm). Moreover, this device also showed a fast response speed (Figure 3d): the rise and decay times are 4 and 9 s for $V_{ds} = 8$ V and $V_{gate} = -70$ V, respectively.

In addition to TMDC layered materials, black phosphorus (donated as "phosphorene") is the latest developed layered material with a tunable direct bandgap ranging from the visible to IR regime.[60] Therefore, the tunable bandgap can be adjusted simply by varying the number of phosphorene layers, making it easier to design devices to an exact working wavelength.[109] Moreover, similar to graphene, phosphorene is usually prepared by a mechanical exfoliation method with a high mobility. In consideration of its numerous unique photoelectric and mechanical properties, phosphorene has appealed to many researchers to explore new photoelectric devices, especially photodetectors. [58,110–113]

Figure 4 demonstrates the fast and broadband photoresponse of phosphorene field-effect transistors reported by Buscema et al.[110] The measured height of the phosphorene flake (Figure 4a) is 8 nm, which corresponds to 15 monolayers of phosphorene. The relationship between the source–drain voltage (I_{ds}) and the gate voltage (V_g) in Figure 4b indicates that the natural doping of this phosphorene is p-type. Specifically, this device exhibits a high on/off ratio of larger than 10^3 and its responsivity is 4.8 mA W^{-1} at a small source–drain voltage bias of 200 mV and 640 nm. The rise and fall times are as short as 1 ms and 4 ms, respectively (Figure 4c). Compared with other layered materials, this phosphorene-based photodetector exhibits a smaller bias but a higher responsivity, faster response times, and a broader detection range. These advantages make phosphorene a very promising material for photodetection, with room for improvement through further device design.

It is known that p–n junctions are the basic building blocks of modern semiconductor devices. It possible to solve the considerable problems of controlling the fundamental parameters inside semiconductor crystals and devices, such as the bandgap, the effective mass of the charge carriers, and the mobility, as well as the refractive index, electron energy spectrum, etc.[114] Therefore, it is of importance for 2D layered materials to construct p–n diodes for practical applications. As shown in **Figure 5**a, Deng et al. demonstrated a heterojunction p–n diode based on phosphorene-monolayer MoS_2 through van der Waals forces with excellent current-rectifying characteristics.[58] Meanwhile, the 2D p–n diode (Figure 5b,c) shows a strong photoresponse and dependence on the incident power (633 nm He–Ne laser). By applying a large negative back gate voltage (–40 V) to modulate the band alignment of the MoS_2 and phosphorene, the ratio of the illumination current over the dark current ($I_{illumination}/I_{dark}$) can be increased to 3×10^3. This is ca. 100 times larger than that of MoS_2 photodetectors due to a better suppression of I_{dark} by the reverse-bias p–n diode.[108] In addition, the responsivity reaches 1.27 A W^{-1} and 11 mA W^{-1} for

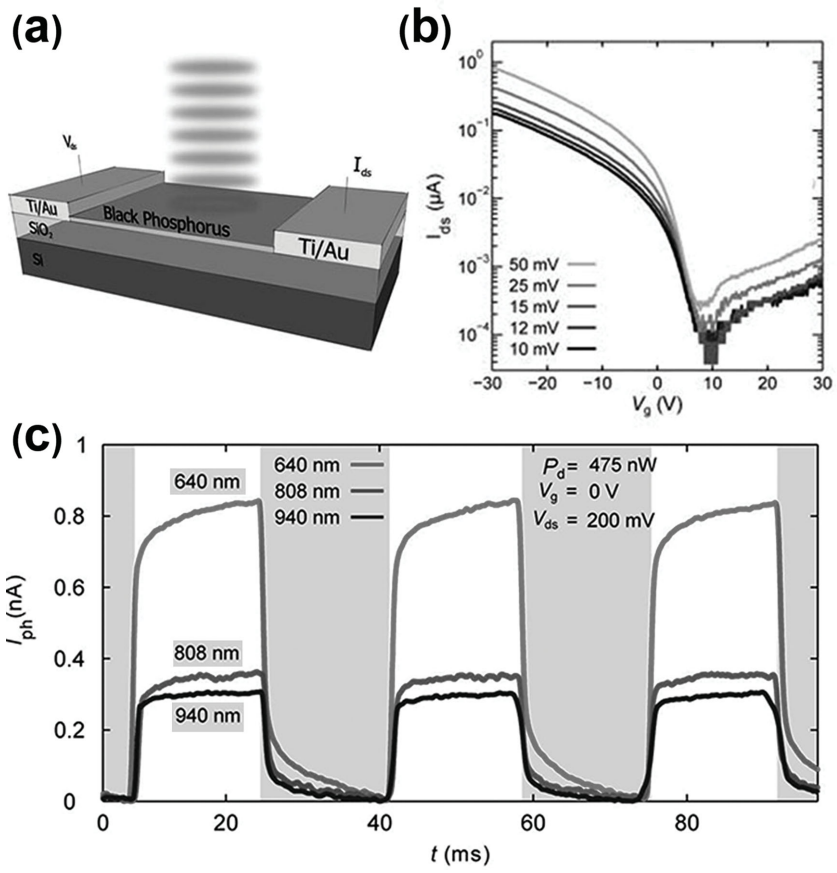

Figure 4. Fast and broadband photoresponse of phosphorene field-effect transistors. a) Schematic of device architecture of phosphorene device. b) Semilog plot of the source–drain current (I_{ds}) versus gate voltage (V_g) of the phosphorene-based FET at the indicated source–drain voltages. c) Temporal photoresponse of the device under different light wavelengths and irradiation energy powers. Reproduced with permission.[110] Copyright 2014, American Chemical Society.

forward and reverse bias, respectively. The maximum responsivity in our devices is up to 3.54 A W^{-1} with the voltage (V_d) applied across the diode at 2 V and 418 mA W^{-1} (at $V_d = -2$ V) under 1 μW laser power (633 nm), respectively, which is nearly 100 times higher than that of a recently reported black-phosphorus phototransistor and 4.8 times higher than that of a carbon-nanotube (CNT)–MoS_2 p–n diode with a much smaller V_d.[115]

2.1.2. Nanofilm-Based Photodetectors

Besides 2D layered materials, solid-state thin films fabricated from various semiconductor materials are alternative platforms for constructing photodetectors. In the past few decades, various sophisticated techniques, such as metal–organic chemical vapor deposition (MOCVD), molecular beam epitaxy (MBE), pulsed laser deposition (PLD), atomic layer deposition (ALD), and magnetron sputtering have been developing rapidly, which has provided vast opportunities for thin-film-based materials, especially GaN, and GaAs based photodetectors, to be successfully commercialized.[36,43,44] However, fabricating photodetectors focusing on the aforementioned techniques usually requires high operating costs, which will hamper further scale-up production of such photoelectric devices. Therefore, it is of great importance to explore novel and facile techniques for fabricating high-performance photodetectors with low cost.

Recently, photodetectors based on closely packed nanofilms have attracted extensive attention from scientists, and a variety of low-cost and effective fabricating approaches, such as spin-coating, electrospinning, vacuum filtration or spraying, and interfacial self-assembly, etc.,[116,117] have been developed in recent years. Amongst these fabrication processes, the solution-based self-assembly of nanostructures is a fashionable and fruitful paradigm for the fabrication of nanofilms. As illustrated in **Figure 6**, typical nanofilms used for photon detection are usually fabricated by oil–water interfacial self-assembly or template-assisted self-assembly methods. Compared with the previously reported strategies, these novel strategies are not only low cost and highly efficient, but are also simple and universal for many kinds of nanostructured materials (samples are listed in the right side of Figure 6), which provides additional opportunities to construct self-assembly hydrophilic nanostructures (nanorods,[118] nanocubes,[119] nanoplates,[56] hollow spheres,[120] etc.) into ultra-thin nanocrystalline films as the active layers of photodetectors. To describe the photodetectors based on nanofilms vividly, Zn_2SnO_4 nanocubes and SnO_2 nanonet nanofilms constructed via the interfacial self-assembly strategy are illustrated first, and further analysis is mainly focused on their optoelectronic properties and applications in photodetectors.

As shown in **Figure 7**a, Wu and co-workers[119] proposed a novel kind of Zn_2SnO_4-nanocube-based monolayer nanofilm, fabricated by the oil–water interfacial self-assembly method. From the SEM image, it can be found that the closely packed Zn_2SnO_4 nanocubes are dispersed regularly on the substrate, and the average edge length of the uniform and semitransparent Zn_2SnO_4 nanocubes is around 650 nm. It is noteworthy that the optical bandgaps of the Zn_2SnO_4-nanocube-based films can be tuned by using different synthetic approaches, along with the associated morphology.[119] In this work, the optical absorption edge could be modulated artificially in the range of 3.18 – 3.54 eV by different heat-treatment processes, which is suitable for UVA (320–400 nm) light detection. This was confirmed by *I–V* measurements of the nanofilm photodetector under different conditions. As shown in Figure 7b, the current density increased more drastically when the device was illuminated by UV light (350 nm) than that in the visible region (550 and 450 nm). To further demonstrate that Zn_2SnO_4 is a promising candidate material for fabricating UV photodetectors, the authors characterized a series of responsivity properties of the device. Compared with previously reported

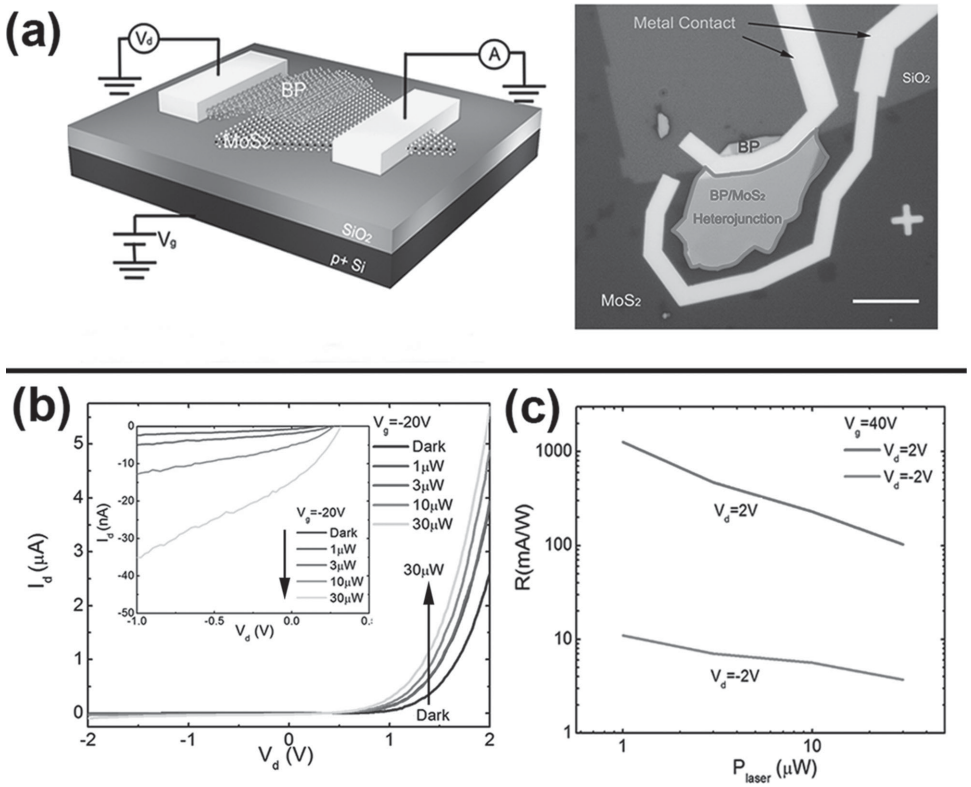

Figure 5. Phosphorene–monolayer MoS_2 van der Waals heterojunction p–n diode. a) Schematics and optical image of the device structure. a p^+ silicon wafer capped with 285 nm SiO_2 is used as the global back gate and the gate dielectric. Phosphorene flakes were exfoliated onto monolayer MoS_2 in order to form a van der Waals heterojunction. Ni/Au electrodes were deposited as contacts. During the electrical measurements, a voltage V_d is applied across the device. The voltage bias V_g is applied to the back gate. Scale bar is 10 μm. b) *I–V* characteristics of the p–n diode under various incident laser powers. The inset shows the details in the reverse bias region. c) Photodetection responsivity (*R*) calculated as a function of incident power. The responsivity decreases as the power increases Reproduced with permission.[58] Copyright 2014, American Chemical Society.

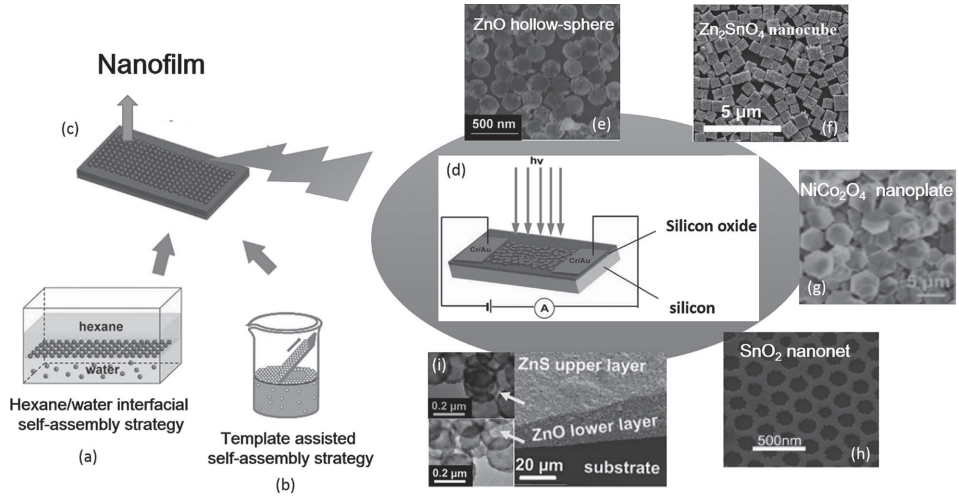

Figure 6. Schematic illustration of the fabricating nanofilm photodetector by a hexane/water interfacial self-assembly strategy. Reproduced with permission.[56,119–122] d,g) Copyright 2011, Wiley-VCH; b,h) Copyright 2012, Wiley-VCH; e) Copyright 2011, Wiley-VCH; a,c,i) Copyright 2012, WILEY-VCH; f) Copyright 2014, Nature Publishing Group.

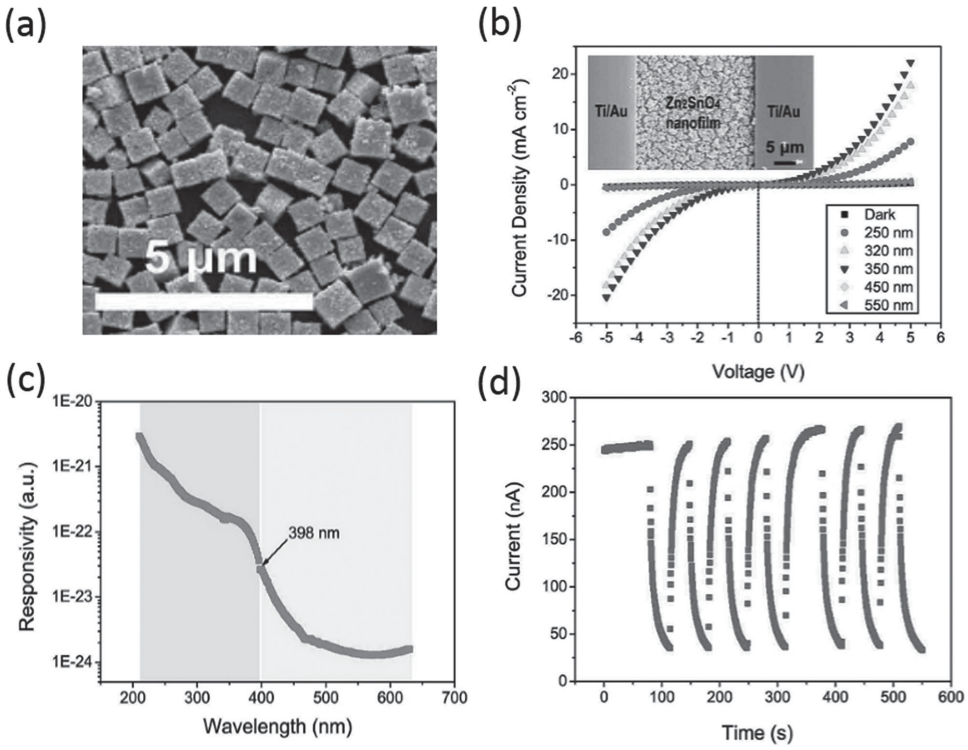

Figure 7. Bandgap tunable Zn_2SnO_4 nanocubes UV photodetector. a) SEM image of the Zn_2SnO_4-nanocube-based film. b) The *I–V* characteristics of the device illuminated with different-wavelength lights or under dark conditions. The inset is an SEM image of the device. c) Spectral photoresponse of the device as a function of wavelengths. d) The reproducible on/off switching upon 350 nm light illumination. Reproduced with permission.[119] Copyright 2014, Nature Publishing Group.

individual-nanostructure-based UV-light photodetectors, it exhibits a much higher photocurrent (43.2 nA at 5 V) and a relatively larger ratio (76) of the illumination current over the dark current. Furthermore, the stable and repeatable time-dependent photoresponse of the as-constructed device (Figure 7c,d) demonstrates that the Zn_2SnO_4-nanocube-based film photodetector fabricated by the interfacial self-assembly method is indeed promising for UV-A radiation detection.

Besides the oil–water interfacial self-assembly fabrication procedure, a colloid crystal polymer template assisted self-assembly method is an alternative avenue for fabricating monolayer nanofilms. Up to now, this method has been developed to fabricate several kinds of 2D ordered nanofilms, such as SnO_2, TiO_2, ZnO, and SiO_2, etc.[123] To estimate the photoelectronic properties of the nanofilm fabricated by the aforementioned strategy, a SnO_2 nanonet was taken as an example for demonstrating its promising applications in photodetectors. **Figure 8**a shows an SEM image of the regular monolayer SnO_2 nanonet fabricated by the aforementioned method. The authors then launched a series of tests of the nanonet-based photodetectors, such as *I–V* characterization under various conditions, the spectral photoresponse as a function of wavelength, and the time-dependent photoresponse. As shown in Figure 8b–d, this device presents several excellent photoelectric properties: high photocurrent (375.2 μA at 1 V), low dark current (89.9 μA at 1 V), and good stability and reproducibility, which is attributed to the regular-structured SnO_2 nanonet. Therefore, the facile method for fabricating regularly structured nanofilms proposed herein could be extended to various building blocks of 2D photonic crystals or optical microcavities. This will open a number of additional opportunities for constructing novel photodetectors with high performance.

2.2. 1D Nanostructured Photodetectors

One-dimensional (1D) nanostructured materials, such as nanowires, nanobelts, and nanotubes, have been attracting a great deal of research interest in recent years due to their unique properties and their potential to revolutionize broad areas of nanotechnology since Iijima found carbon nanotubes[124] and Wang's group first synthesized inorganic semiconducting oxide nanobelts.[125] Compared with 2D nanostructured materials, having 1 dimension limited within the nanoscale, 1D nanostructured materials possess an additional spatial dimension – in total 2 dimensions confined within the nanoscale. Therefore, they are additional ideal systems for exploring a large number of novel phenomena at the nanoscale, as well as investigating the size and dimensionality dependence of properties for potential applications.[126] In particular, taking advantage of the large surface-to-volume ratio and Debye length comparable to their sizes, photodetectors based on 1D nanostructured materials have become one of the most attractive photoelectronic devices in recent years. Considering the extremely small size of nanostructured materials, a highly controlled method with excellent accuracy is usually needed to fabricate individual

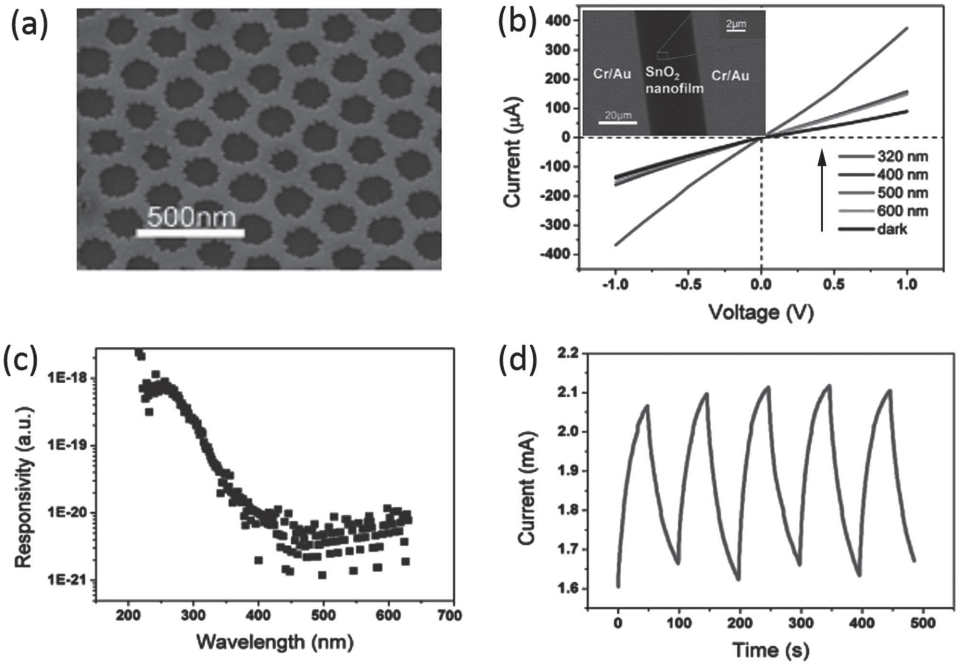

Figure 8. SnO_2 monolayer nanofilms based UV photodetectors. a) The SEM images of 2D ordered SnO_2 monolayer nanofilms obtained using polymer spheres with a size of 228 nm. b) Spectral photoresponse of the device measured at a bias of 5.0 V at diffraction wavelengths ranging from 210 to 630 nm. c) *I–V* characteristics of the device illuminated with different wavelength lights and under dark condition; the inset is an SEM image of the photoresponse device based on the 2D ordered SnO_2 monolayer nanofilm, the electrodes distance is ca. 1.5 μm. d) Time-dependent response of the photodetector measured under air conditions at a bias of 5.0 V, and the light power intensity was 0.91 mW cm^{-2}. Reproduced with permission.[121] Copyright 2012, Wiley-VCH.

nanowires, nanotubes, or nanobelts into nanoscale photodetectors, and preparing them into assemblies through a simple procedure can be an alternative for fabrication of photodetectors. Therefore, recent developments of 1D nanostructured photodetectors are reviewed in this section with an emphasis on the methods for device fabrication.

2.2.1. Individual 1D Nanostructured Materials for Photodetectors

Taking advantage of the numerous facile fabrication processes of monodisperse 1D nanostructures, one of the most commonly used ways to fabricate 1D nanostructured materials into photodetectors is to combine them on a flat substrate with electrodes by the electron-beam deposition and photolithography technique.[127] As an example, Liu et al. recently fabricated a new UV-A photodetector based on $K_2Nb_8O_{21}$ nanowires.[128] An SEM image of a photodetector based on a single $K_2Nb_8O_{21}$ nanowire is shown in **Figure 9**a. The $K_2Nb_8O_{21}$ nanowires in this work were synthesized using a facile molten method by taking Nb_2O_5 powder and molten KCl as raw materials at 900 °C for 3 h in a conventional horizontal furnace. The as-synthesized $K_2Nb_8O_{21}$ nanowires have a main distribution width and length of 130 nm and 20 μm, respectively. The single-crystal nature of the nanowires and [001] growth direction were further confirmed by high-resolution transmission electron microscopy (HRTEM) and selected area electron diffraction (SAED).

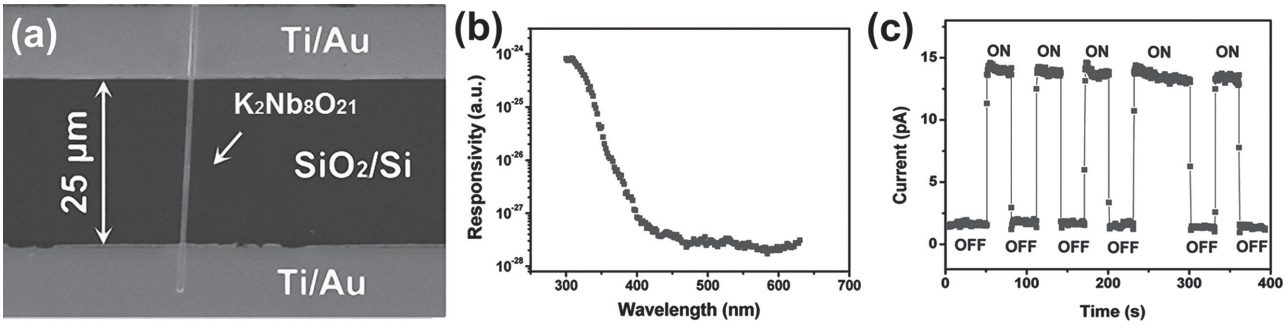

Figure 9. UV-A photodetector based on individual $K_2Nb_8O_{21}$ nanowires. a) SEM image of the single-nanowire photodetector. b) Spectral response of the photodetector as a function of wavelength from 630 to 300 nm under 5 V bias. c) Current–time response of the photodetector illuminated with 320 nm light measured using a mechanical chopping method at 5 V. Reproduced with permission.[128] Copyright 2014, Wiley-VCH.

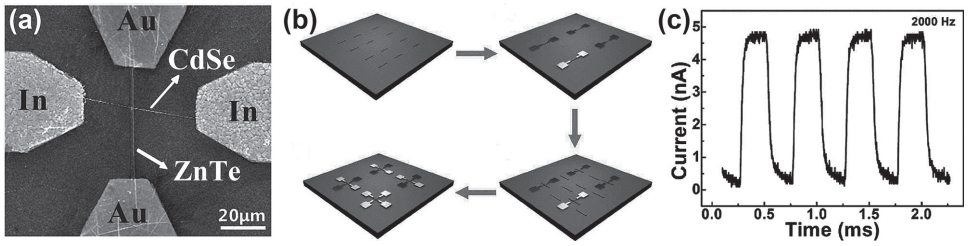

Figure 10. White light photodetector based on crossed p-ZnTe/n-CdSe NR heterojunction. a) SEM image of a p-ZnTe/n-CdSe NR heterojunction photodetector. b) Schematic illustration of the process used to fabricate p-ZnTe/n-CdSe NR heterojunction photodetectors. c) Photoresponse characteristics of the heterojunction photodetector to pulsed white-light irradiation at frequencies of 2000 Hz. Reproduced with permission.[141] Copyright 2014, Royal Society of Chemistry.

Owing to the bandgap of $K_2Nb_8O_{21}$ being approximately 3.1 eV, the photodetector exhibits an excellent wavelength selectivity for UV-A light detection with a sharp cut-off edge at ca. 400 nm. As shown in Figure 9b, a UV (300 nm)–visible (500 nm) rejection ratio of more than 3 orders is achieved in the spectral response, indicating that the as-prepared device is a "visible-blind" photodetector. The time response characteristics of this photodetector shown in Figure 9c imply that the current change between light-on and light-off takes place upon 320 nm light illumination at an applied voltage of 5 V with a short rise/decay time of less than 0.3 s. The calculated responsivity (R_λ) and external quantum efficiency (EQE) of this photodetector were as high as 2.53 A W^{-1} and 982%, respectively at the wavelength of 320 nm under 5 V bias. From all this mentioned above, it is concluded that these $K_2Nb_8O_{21}$ nanowires are a promising candidate for fabricating photodetectors with superior response speed, spectrum selectivity, and sensitivity.

Similar to $K_2Nb_8O_{21}$ nanowires, many other materials, including $InAs_xP_{1-x}$,[129] ZnSe,[50] Cd_3P_2,[69] In_2Te_3,[130] Nb_2O_5,[131] InAs,[132] SnO_2,[133] etc., have recently been fabricated successfully into individual 1D nanostructured photodetectors. Moreover, to improve device performance, individual 1D nanostructured materials can also be used to construct novel hybrid nanostructures, including core–shell nanocables,[134–136] biaxial nanobelts,[137,138] single-heterojunction nanowires,[139] and lateral heterostructures,[140] which often exhibit superior optoelectronic properties with a multitude of additional functions compared with the pure component.

Figure 10a shows a SEM image of white light photodetectors based on crossed p-ZnTe/n-CdSe nanoribbon (NR) heterojunctions.[141] Both the p-ZnTe and the n-CdSe NRs were synthesized via a co-thermal evaporation method as single crystals, which was confirmed by HRTEM and SAED. The stepwise procedure for the construction of the p-ZnTe/n-CdSe NR heterojunction photodetectors is by a contact printing technique (Figure 10b).[142] In this regard, it has two major steps: firstly, the as-synthesized ZnTe NRs were dispersed in parallel on a SiO_2 (300 nm)/p^+-Si substrate by a contact printing technique, followed by the deposition of Au electrodes; secondly, CdSe NRs were then dispersed on the substrate with an orientation perpendicular to the ZnTe NRs, followed by the deposition of indium electrodes. Consequently, the CdSe NRs crossed on the ZnTe NRs heterojunctions were completed in this situation, and several characterizations of the photoelectronic properties were carried out as follows. The n-type conductivity of the CdSe NRs and the p-type conductivity of the ZnTe NRs were evidenced by charactering the source–drain current (I_{ds}) versus source–drain voltage (V_{ds}) properties of individual NRs on SiO_2 (300 nm)/p-Si substrates, respectively. The as-fabricated device showed a rectification ratio up to 10^3 at ±5 V, and a low turn-on voltage of 2.6 V in the dark. As shown in Figure 10c, the p-ZnTe/n-CdSe photodetector shows an excellent stable and reproducible photoresponse under pulsed white-light illumination. In addition, the rise time and fall time were determined to be 37 and 118 μs, respectively, at a reverse bias voltage of −2 V, which was much quicker than previously reported ZnTe- and CdSe-based nano-photodetectors.[141] Therefore, thanks to the meticulously designed procedures and particular adaptability of 1D nanostructured materials, it is believed that the device fabrication process discussed in this section will become one of the most useful methods for 1D nanostructured photodetectors, especially contributing to fabricating prototype devices for researching their basic photoelectronic properties.

2.2.2. Assemblies of 1D Nanostructured Materials for Photodetectors

Construction of photodetectors based on individual 1D nanostructures is often expensive and time-consuming. To achieve good control of device structure, photolithography or electron-beam lithography (EBL) is indispensable, and the efficiency of device preparation is relatively low. For photolithography, 1D nanostructured materials are often randomly dispersed and may be damaged by the lift-off process, while for EBL, the device fabrication process is much more complicated and time-consuming. On the other hand, additional complicated procedures may be needed to integrate photodetectors based on individual 1D nanostructures with other photoelectronic elements due to their small sizes and weak photosignals. Thus, a possible way to make sure that photodetectors based on 1D nanostructured materials arrive at a practical standard, may be preparing the nanowires, nanotubes, or nanobelts into assemblies in the form of disordered networks or orientated arrays through a simple fabrication procedure. Here, we describe two kinds of assemblies of nanostructured materials for photodetectors.

Figure 11 shows a THz detector working at room temperature, which is based on an array of highly aligned and ultralong single-wall CNTs developed by He et al.[143] The CNTs in

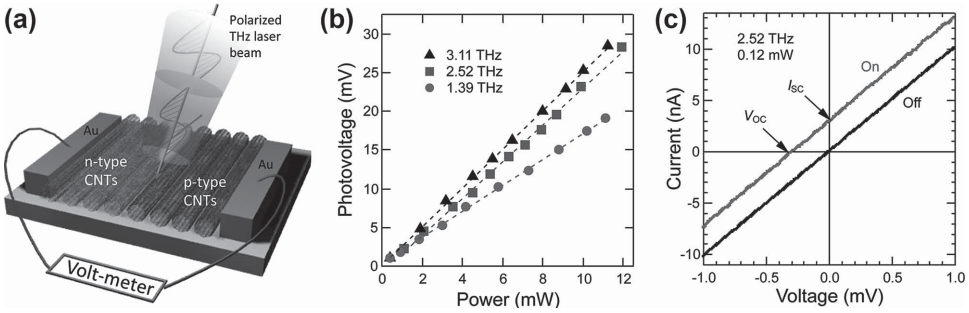

Figure 11. THz detector working at room temperature based on an array of single-wall CNTs. a) A schematic diagram of the experimental geometry. The *I–V* characteristics are measured under the illumination of a linearly polarized THz beam in air at room temperature. b) Power dependence of V_{OC} for frequencies of 1.39 THz, 2.52 THz, and 3.11 THz. c) *I–V* characteristics under illumination by a THz beam with a frequency of 2.52 THz (red) and without illumination (black). Reproduced with permission.[143] Copyright 2014, American Chemical Society.

this work were grown vertically from a single line of catalyst particles on a silicon substrate by chemical vapor deposition (CVD) and the ratio of semiconducting and metallic single-wall CNTs is about 2:1. The CNT arrays had a typical height of ca. 150 μm and their width was about 2 mm, which was decided by the length of the catalysts. The as-synthesized CNT arrays film was then transferred onto Teflon (which means that this THz detector has potential in flexible electronics) or AlN substrates, and gold contact electrodes were deposited at the ends of the film by electron-beam evaporation to complete the devices. A p–n junction was created by partial doping of the CNT film and the CNTs were aligned perpendicular to the direction of current flow (Figure 11a). As shown in Figure 11b, the as-prepared terahertz detector shows high responsivity values over a wide range of THz radiation (2.5 V W^{-1}, 2.4 V W^{-1}, and 1.7 V W^{-1} at 3.11 THz, 2.52 THz, and 1.39 THz, respectively). The *I–V* curve with and without THz radiation at 2.52 THz is shown in Figure 11c. It was found that the device could generate a finite short-circuit photocurrent (I_{SC}) and open-circuit photovoltage (V_{OC}) at zero bias, which makes it possible for it to function as a powerless THz detector. In addition, the photosignal of this THz detector is strongly dependent on the polarization of the incident THz wave, which mainly arises from the intrinsic polarization-dependent absorption of the CNTs in this work. The parallel-to-perpendicular ratio of the incident THz wave with respect to the nanotube alignment direction is about 5:1. The macroscopic size and the relatively simpler device fabrication procedure, as well as the high responsivity of this THz detector compared with detectors based on individual 1D materials, make these very promising for THz detection.

In addition to the horizontal p–n CNT arrays, Tsai et al. proposed an alternative avenue to build photodetectors with a high broadband responsivity by using ZnO vertical nanorod arrays (NRAs) on a Si substrate to absorb UV photons effectively in the short-wavelength region and facilitate more photons getting into the photodetectors in the long-wavelength region, as an anti-reflective layer.[144] As can be seen in the schematic of this device (**Figure 12**a), a 100-nm-thick SiO_2 passivation layer was deposited before growth of the ZnO NRAs using plasma-enhanced CVD. Large-scale and well-aligned ZnO NRAs were then prepared using a low-temperature hydrothermal method after deposition of a 100-nm-thick ZnO seed layer on the prepared substrate. Further characterization by X-ray diffraction (XRD) and HRTEM confirms that the ZnO NRAs were hexagonal wurtzite-structured single crystals and that they grew along the [0001] direction. Figure 12b shows the *I–V* characteristics of metal–semiconductor–metal (MSM) photodetectors with and without 543 nm laser under a 15 V bias. It could be found that the photocurrent-to-dark-current contrast ratio of this Si MSM photodetector was increased by 2 orders of magnitude by introducing ZnO NRA layers. This is because that the leakage current of the photodetector could be reduced efficiently by the insulating SiO_2 layer in dark conditions, while the anti-reflective ZnO NRA structures (the green light at 543 nm is not absorbed by the wide-bandgap ZnO) create more opportunities for generating a photocurrent in Si MSM photodetectors.

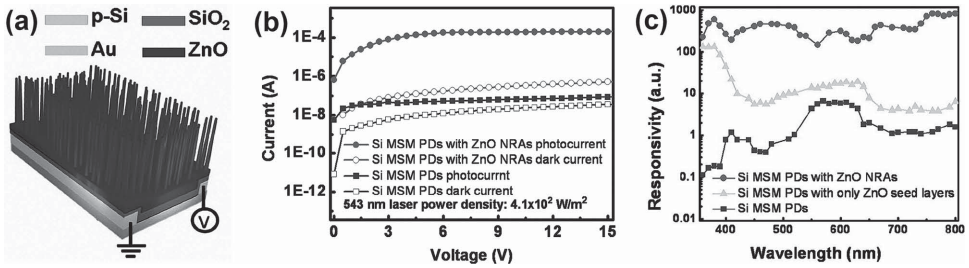

Figure 12. Si MSM photodetector (PD) with ZnO NRAs exhibiting ultrahigh broadband responsivity. a) Schematic of the Si MSM PD with ZnO NRAs. b) *I–V* characteristics of the Si MSM PDs with and without ZnO NRAs measured in the dark and under illumination (543 nm). The incident light power density is 4.1×10^2 W m^{-2}. c) Spectral responsivity of Si MSM PDs, Si MSM PDs with only ZnO seed layers and Si MSM PDs with ZnO NRAs as a function of the wavelength under 15 V bias. Reproduced with permission.[144] Copyright 2011, American Chemical Society.

In addition, because a high electric field can facilitate the tunneling of UV photogenerated carriers through a thin SiO_2 layer, the responsivity of the photodetector with ZnO NRAs increased by 3 and 2 orders of magnitude in the UV and vis/NIR regions compared with a pristine Si photodetector (Figure 12c). This study provides an efficient method for the potential application of 1D nanostructured assemblies in next-generation broadband photodetectors with high gain.

Therefore, in addition to the relatively simple fabrication procedure compared with photodetectors based on individual 1D nanostructured materials, photodetectors based on assemblies of 1D nanostructured materials also have the potential to achieve an enhancement of sensitivity, photocurrent intensity, and stability. For instance, a variety of other assemblies based on 1D nanostructured materials, including disordered networks,[27,145–147] orientated arrays,[148–150] nanowire bridges,[151] nano-branched arrays,[152] multilayered nanobelts,[153] top-down etched arrays,[154] and roll-to-roll assembled CNT networks,[155] have been fabricated into photodetectors showing outstanding properties. Thus, preparing 1D nanostructured materials into assemblies is one of the most important methods to construct 1D nanostructured materials into photodetectors for practical applications.

2.3. 0D Nanostructured Materials for Photodetectors

Zero-dimensional (0D) nanostructured materials usually refer to materials whose excitons are confined in all three spatial dimensions (<100 nm). The nanoscale confinement of 0D materials makes it possible to tune its energy band by its size and shape. As a result of this 3D tunability of 0D materials, they usually exhibit several unique electronic and optical properties, especially for use of photodetectors.[156,157] In addition to the tunable bandgap, 0D materials also share a large specific surface area, which makes them more suitable than higher dimensional materials like bulk materials or 1D materials for obtaining a higher light absorption efficiency. High-photoabsorption 0D materials can be sensitively combined with other materials to achieve high-performance photodetectors. In recent years, many novel photodetectors have been proposed based on newly processed 0D materials, especially quantum-dot (QD)-based materials with different structures. In this section, recent advances in direct photodetection with QD materials, QD sensitized detectors, and QD–2D hybrid detectors are reviewed in detail.

2.3.1. Photodetectors Built Directly on QD Materials

As a quasi-zero-dimensional material, QDs such as GaAs,[158] Ag_2Te,[159] HgTe,[37] PbS,[160–162] CdS,[163] CdSe,[164] and PbSe,[165,166] as well as graphene quantum dots (GQDs)[39,167,168] etc. are usually fabricated by the high-temperature droplet epitaxy technique, solution processing, and so on, and they can be directly used to build photodetectors. The performance of such devices is bound up with their preparation methods. For instance, QDs grown directly on a solid wafer by MBE can be easily used to fabricate photodetectors;[158] however, the cost is relatively high for the wide application of this method. Therefore, to balance the trade-off between the performance of a device and the fabrication cost, a study of inorganic QD arrays using solution processing might be an alternative avenue.[169] In the following sections, examples of high-performance photodetectors based on QDs that have a low cost will be described.

As shown in **Figure 13**a,b, Lee et al. developed a novel low-cost QD-based field-effect transistor by using CdSe nanocrystals capped with molecular $[(N_2H_4)_2(N_2H_5)_2In_2Se_4]$ metal-chalcogenide-complex (MCC) $In_2Se_4^{2-}$ nanocrystals.[169]

Amazingly, after organic molecules at the surface of CdSe and CdSe/CdS core–shell nanocrystals were displaced by MCCs, the electron mobility (μ_e) could be improved by several orders of magnitude: about an order of magnitude higher than that of the best solution-processed organic and nanocrystal devices (Figure 13c).[170] In addition, the authors also used CdSe/CdS core–shell nanoparticles with $In_2Se_4^{2-}$ ligands to build photodetectors. Then, they measured the responsivity of the devices at different monochromatic illumination (Figure 13d). It is noteworthy that the responsivity of the CdSe/CdS core–shell device could achieve as high as 260 A W^{-1} under 0.5 V bias voltage at a wavelength of 450 nm (0.65 mW cm^{-2}), and the normalized detectivity D^* was more than 1×10^{13} Jones (1 Jones = 1 cm $Hz^{1/2}$ W^{-1}) (Figure 13e).

Beyond the outstanding photodetectors based on the aforementioned semiconductor QD materials, constructing low-dimensional photodetectors by using nontoxic graphene quantum dots (GQDs), which have many attractive optical and electric properties, has drawn a lot of attention recently. GQDs are small graphene fragments whose excitons are confined in all three dimensions. Hence, unlike 2D layered graphene, their bandgap can be tuned by the size itself, as well as by edge modification of the functional groups. This allows it to detect not only a broad spectrum,[39,171] but also certain regions of light with high detectivity,[167] as shown in **Figure 14**, which shows a sketch of a GQD-array photodetector.[19] This broadband and high-photoresponse photodetector was fabricated as follows. First, a mechanically exfoliated graphene monolayer field-effect transistor (FET) was created on a SiO_2/Si substrate. Then, a titanium (Ti) sacrificial thin layer was deposited on top of the graphene. After the Ti layer was etched away, GQD arrays with different GQD sizes were formed on the substrate, depending on the thickness of the Ti layer. In this work, Zhang et al.[96] demonstrated that the GQD arrays can not only act as electron trapping centers on the boundary, but also create a bandgap due to quantum confinement. Therefore, a very high photoresponsivity and ultra-wideband photoresponse was achieved through this band-structure engineering. The *I*–*V* curves of the device with and without 532 nm illumination are presented in Figure 14b; a photoresponsivity as high as 8.61 A W^{-1} was achieved at V_D = 0.1 V (drain–source voltage). This value of responsivity is roughly 800 times more sensitive than previous graphene photodetectors, and around 10 times more sensitive than the CMOS-based sensors in today's digital cameras.[172] The photocurrent can also be modulated by the gate voltages (Figure 14c). Moreover, a comparison of the time-dependent photocurrent between the pristine and processed graphene devices (Figure 14d) further demonstrated that the devices share both the advantages of high photoresponsivity and

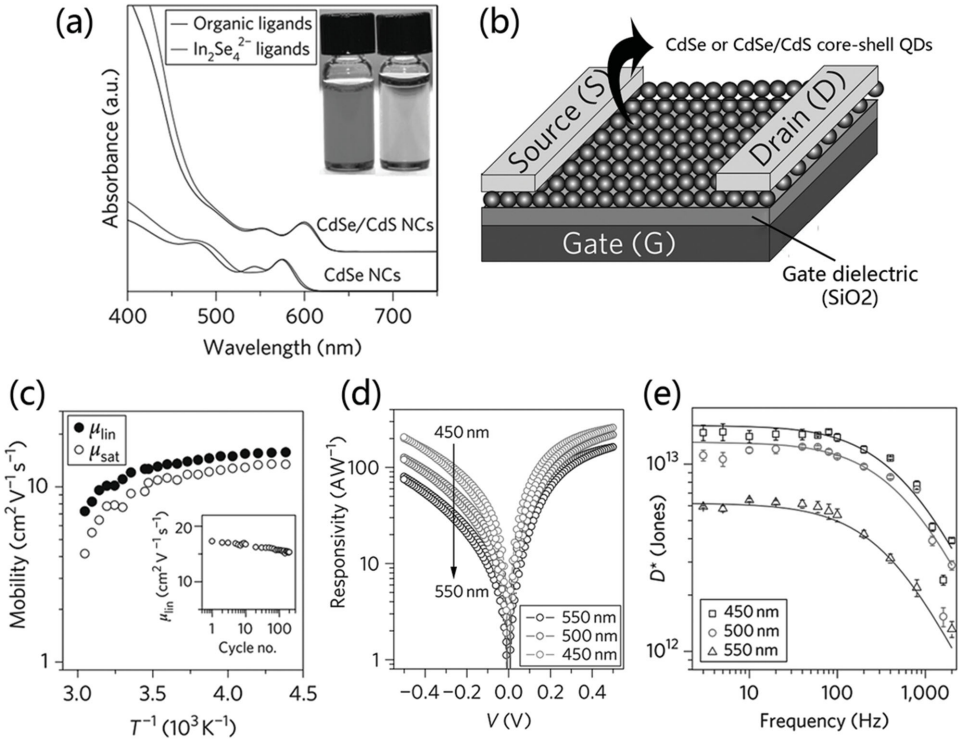

Figure 13. Photodetectors of QD materials. a) Absorption spectra for 4.6 nm CdSe nanocrystals and 10.0 nm CdSe/CdS core–shell nanocrystals capped with original organic capping ligands in hexane (black lines) and capped with $In_2Se_4^{2-}$ in hydrazine (blue lines). Inset: photographs of colloidal solutions of CdSe (left) and CdSe/CdS (right) nanocrystals capped with $In_2Se_4^{2-}$. b) Schematic of field-effect transistors using $In_2Se_4^{2-}$-capped CdSe or CdSe/CdS nanocrystals. c) Temperature dependence of field-effect mobility for an n-channel FET assembled from $In_2Se_4^{2-}$-capped 3.9 nm CdSe nanocrystals. Inset: evolution of field-effect mobility over 200 consecutive cycles of the gate voltage between −30 V and +30 V at V_{DS} = 2 V. The nanocrystal layer was annealed at 200 °C for 30 min (L = 72 mm, W = 954 mm). The thickness of the SiO_2 gate dielectric was 100 nm. d) Responsivity of a 60-nm-thick layer of $In_2Se_4^{2-}$-capped CdSe/CdS core–shell nanocrystals with 2.9 nm CdSe cores and 2.6-nm-thick CdS shells at different wavelengths measured at 5 Hz light-modulation frequency. e) Frequency dependence of the normalized detectivity D^*, measured under 21 V for a device using $In_2Se_4^{2-}$-capped CdSe/CdS core–shell nanocrystals annealed at 150 °C for 30 min. The 3 dB bandwidth is ca. 0.4 kHz. Reproduced with permission.[169] Copyright 2011, Macmillan Publishers Limited.

reliability for as-designed photodetectors. Although this device can only work at low temperature (150 K), the above photodetectors made from pure GQD arrays have very wide broadband and high photoresponsivity features, which provides an additional platform for building a photodetector on the nanoscale.

2.3.2. Hybrid QD Photodetectors

As mentioned above, QD materials can not only play an important role as a central component of the photodetector, but also sensitize other forms of materials, including polymers,[162] nanowires,[163] and even quantum dots themselves in the photodetector.[160,161] Therefore, to improve the performance of present low-dimensional photodetectors, it is essential to design hybrid devices integrated with QD nanocrystals.[173–175] As an example, to yield an ultra-high responsivity of photodevices, a special hybrid configuration consisting of 2D–QD materials was put forward. Up to now, some hotly studied areas are focused on 2D layered materials in terms of graphene, black phosphorus, and TMDCs. These single or multilayered 2D materials possess ultra-high carrier mobility (up to 60 000 $cm^2V^{-1}s^{-1}$ for graphene[176] and wide spectral absorption, and have been confirmed to be a new class of building block for photodetectors. To be excited, modified by a layer of QDs, these devices exhibit a higher light-absorption rate. In this QD–2D hybrid structure, additional incident light is absorbed by the QD layer to increase the number of photon-generated carriers that can transfer through the 2D channel with a high electron mobility, leading to a higher quantum efficiency of photodetection.[177–179]

A typical graphene/QDs hybrid photodetector is shown in **Figure 15**a.[177] In this device, the spectral sensitivity could be tuned easily by controlling the size of the QDs (Figure 15b), and the linear dependence of the photocurrent on the drain–source voltage (V_{SD}) reveals that there is an excellent Ohmic contact between the electrodes (source and drain) and the QDs (Figure 15c). Moreover, the responsivity is as high as 5×10^7 A W^{-1} at a wavelength of 600 nm when the back-gate voltage (V_{BG}) is smaller than the charge neutrality point (V_D), corresponding to a photoconductive gain of 1×10^8, which is competitive with epitaxy III–V group semiconductors.[180] In addition, the authors demonstrated that the responsivity of this device could completely fall to zero by tuning the Fermi energy to be close to the Dirac point at V_{BG} = 4 V (Figure 15d), which also represents an excellent back-gate-tunable ultra-high-gain phototransistor.

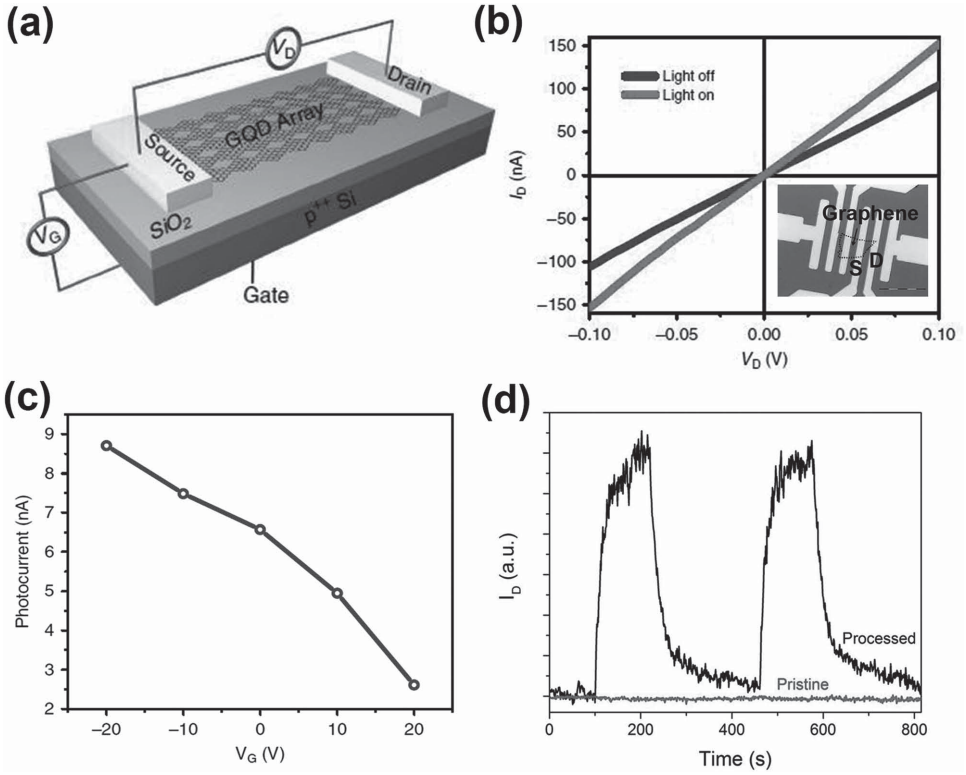

Figure 14. Graphene quantum dots (GQD) array photodetector with broadband and high photoresponse. a) Schematic of GQD device. b) *I–V* curves of device with and without 532 nm illumination. Photoresponsivity of 8.61 A W^{-1} is achieved at a V_D voltage of 0.1 V. The inset shows a microscopy image of the device. c) Gate-voltage dependence of the photoresponse characteristic of device. d) Temporal photoresponse of the pristine and processed graphene device under the excitation of a 532 nm laser at a 100 mV source–drain and zero gate voltage. Reproduced with permission.[96] Copyright 2013, Nature Publishing Group.

In addition to the graphene–PbS QD hybrid phototransistors addressed above, the hybrid combination between MoS_2 and PbS QDs based on same structure was also explored with an ultra-high responsivity of 6×10^5 A W^{-1} (1 V).[40] Moreover, except for traditional semiconductor QDs, broader-spectrum photodetectors with a high wavelength-selective enhancement could be achieved by using GQDs as the active component.[171] **Figure 16**a shows a sketch of a GQD-based hybrid photodetector. In this study, the device is composed of multilayered GQDs sandwiched between two single-layer graphene sheets. On the one hand, most absorption of multiband light takes place in the GQDs because of the multiple scattering of light between the GQDs and the top graphene; on the other hand, it is easy to excite electron–hole pairs and generate a large photocurrent by tunneling carriers through the GQDs. As shown in Figure 16b, it is typical of tunneling diodes. It is noteworthy that, although less light was absorbed by the device at a wavelength of 400 nm, the responsivity still could reach ca. 0.2 A W^{-1} (Figure 16c), which is comparable with those reported for commercial Si and InGaAs photodetectors (ca. 0.5 and ca. 0.9 A W^{-1} at 4.2 K), respectively.[181,182] In addition, the device possessed a fast response speed. It can be found that in Figure 16d, it is the transient photocurrents studied at various bias voltages. The turn-on and turn-off transient responses of the devices are measured to be on the order of microseconds, respectively. This further confirms that fabricating hybrid photodetectors in a junction with QDs is an appealing method to enhance the performance of the present one.

All in all, the aforementioned enormous enhancement of the photodetectors could be achieved by various QDs. Constructing hybrid structures in conjunction with different low-dimensional materials may be an appealing way to realize the simplification and high performance of photodetectors at the nanoscale. However, the performances of these devices still need to be modified for practical applications. Hence, additional new techniques or design concepts are crucial for low dimensional photodetectors to pave the way toward moving outside of lab.

3. Photodetectors with Greater Performance Benefiting from New Techniques

Dating back to a century ago, when photodetectors were invented, many progress milestones have been achieved. Briefly, they mainly boil down to the following two aspects: firstly, diverse commercially available devices have been obtained thanks to the insulating and doping techniques of the semiconductors industry. Secondly, following Moore's law, the size of present photodetectors has shrunk continuously toward the nanoscale for further integration with other photoelectronic elements. Therefore, various nanocrystal solids are considered to be the prospective materials for photodetection.

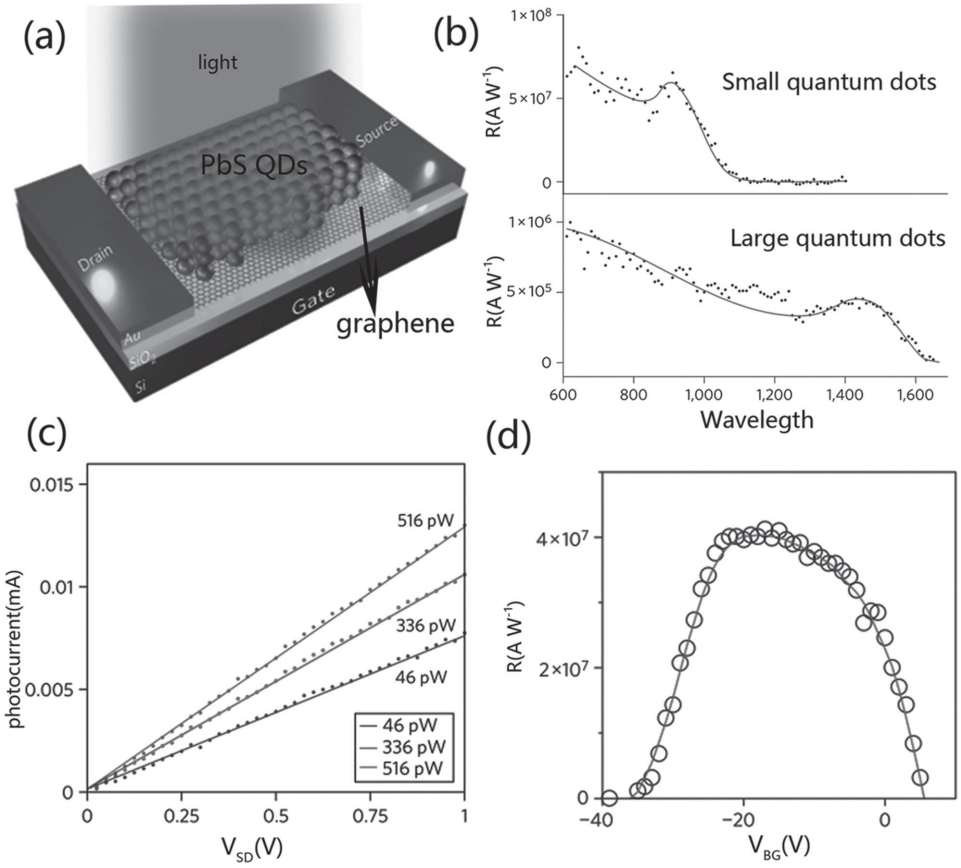

Figure 15. QD-2D hybrid photodetectors. a) Schematic of the graphene–PbS QD hybrid phototransistor. b) Spectral responsivity of two phototransistors with difference in sizes of PbS quantum dots c) Photocurrent of the graphene–quantum-dot hybrid transistor for different optical powers as a function of drain–source voltage (V_{DS}). d) Responsivity as a function of back-gate voltage. Reproduced with permission.[177] Copyright 2012, Macmillan Publishers Limited.

However, as described in the previous paragraph, low-dimensional photodetectors are still at an early stage of development, and their performances need to be improved for practical applications. Besides that, in photodetection system, the size mismatch between the photonic element and the electronic circuitry is still one of the most challenging issues waiting to be resolved. Therefore, the ability to explore new techniques to overcome these problems is essential to realize photodetectors with a greater performance. Fortunately, inspired by some unique physical effects of nanoscale materials, versatile hybrid low-dimensional photodetectors with fascinating performance and amazing functions have been explored recently. In the following section, these two types of devices, as well as their working mechanism, will be discussed in detail.

3.1. Novel Strategies for Fabricating Photodetectors with Advance Functions

As an important parameter of photodetectors, the responsivity directly reflects the photoelectric conversion ability of a device. Therefore, a large amount of work is aimed at improving the optical responsivity of the devices by increasing both the internal and external quantum efficiency. It is not hard to find from previous results that available approaches can be investigated at any stage of the photoelectric-conversion process, including the generation, separation, and transportation of electron–hole pairs. In practical terms, various QD materials have been explored to improve the light absorption of devices (see Section 2.3). Moreover, different gain mechanisms have been employed to improve the responsivity of devices, such as, benefiting from the impact ionization effect of the photogeneration carriers, avalanche photodetectors have become available;[34] owing to the tunnelling effect in inter-sub-band superlattices, resonant tunnelling photodetectors have been obtained;[183] and thanks to minority-carrier traps in the semiconductor, photodetectors with a high photoconductive gain can be achieved.[184] However, among these gains illustrated above, only a photoconductive gain could be achieved easily in nanostructured photodetectors despite the long response time. Resonant tunnelling diodes and avalanche photodetectors usually need sophisticated fabricating techniques to form high-quality crystallization or special interfaces. Hence, common ways to improve the quantum efficiency without sacrificing other properties of the nanodevices are urgently needed. Fortunately, low-dimensional photodetectors with a higher performance based on the plasmon effect and the pizeo-phototronic effect have been explored. Herein, some of them will be covered in the following.

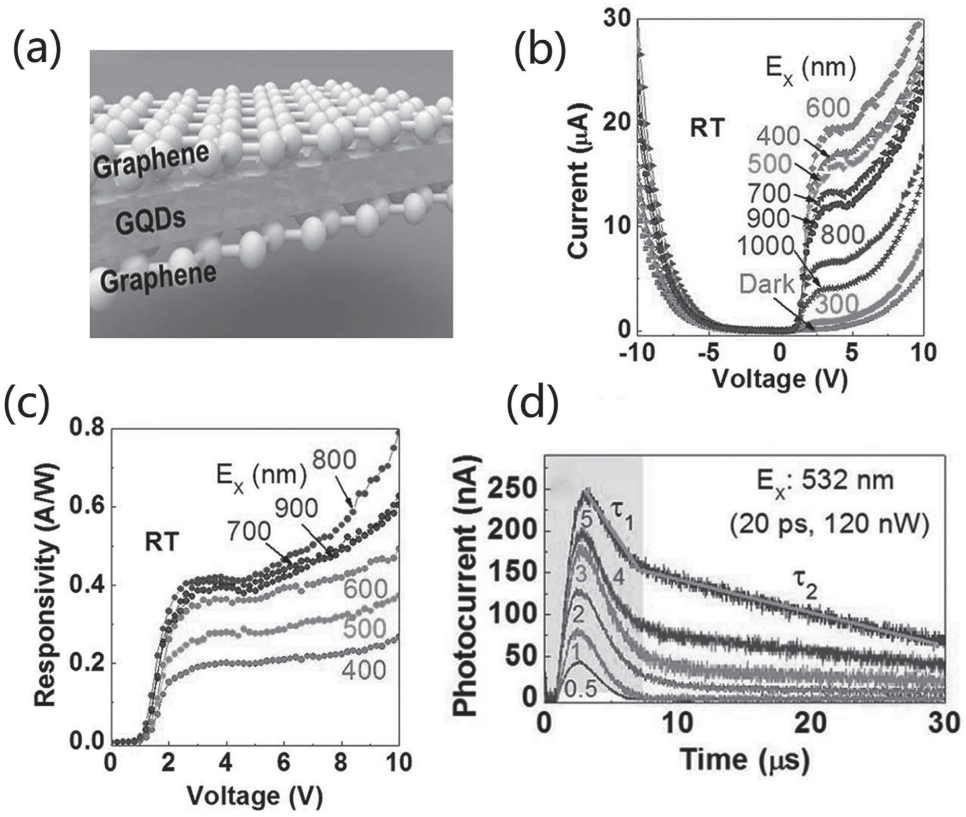

Figure 16. Graphene quantum dots based hybrid photodetector. a) Schematics of a typical GQD photodetector. b) *I–V* characteristics in the dark and under illumination at various photon wavelengths from 300 to 1000 nm. c) Responsivity as a function of forward bias at various photon wavelengths from 400 to 900 nm. d) Short-term photocurrent switching at various bias voltages. Reproduced with permission.[171] Copyright 2014, Macmillan Publishers Limited.

3.1.1. Efficient Light Coupling into Photodetectors by a Designed Plasmonic Nanostructure

Plasmonics is a kind of hybrid electromagnetic wave arising from the collective oscillations of the free electron gas within the metal, which possesses the unique ability of manipulating light at nanometer scales with a high local-field enhancement.[20] This makes it possible to concentrate, and manipulate light at subwavelengths without consideration of the optical diffraction limit, which plays an important role in constructing nanosized photodetector. During the last decade, numerous devices with high responsivity,[185,186] and high speed[187] have been developed, taking advantage of the plasmonic technique. Especially, studies in terms of cavities, waveguides, or antenna, etc. have achieved remarkable effects in the improvement of the device performance.[188–190] These have been described in a previous review,[191] and are not present here. As is well known, to achieve a giant enhancement of photoresponse by surface plasmons, the key factor is their energy match, namely the large frequency overlap between surface plasmons and response peaks. This is a complicated issue, because the surface plasmons are very sensitive to the size, shape, and dielectric properties of the nanoparticles and the dielectric environment.[19,20] Therefore, using suitable plasmonic structures to achieve strong light-focusing at subwavelengths is usually a key avenue to generate plasmonic oscillations at a desired frequency, and many methods have be employed to improve the enhancement effect of photodetectors by tuning of the metallic structures. In this section, we will discuss some schemes of recently developed plasmonics-enhanced devices in view of the responsivity enhancement and wavelength selectivity by different designed types of metallic nanostructures.

A schematic of a quantum-dot infrared photodetector (QDIP) with a gold two-dimensional hole array (2DHA) is shown in **Figure 17**a, which is fabricated using a combination of a standard optical lithography and a metal lift-off process (Figure 17b). To achieve an optimum plasmonic–QD interaction, the authors identified three criteria: firstly, they used "a" (lattice constant) with a suitable size (inset in Figure 17b)[192] to guarantee a good spectral matching of plasmonic resonance to QDs spectral response; secondly, they tuned the diameter *d* of the holes to optimize the 2DHA design, to improve the transmittance to ca. 100%, and then they controlled the thickness of the QD-layer to achieve spatial matching of the vertical extent of the plasmonic field to the QD region. Particularly, the ability to vary the diameter *d* facilitates a strong light transmission through the 2DHA at the resonance wavelength (inset of Figure 17c), leading to a larger absorption enhancement of the active layer, and a 130% absolute enhancement of the IR photoresponse was achieved (Figure 17c). This study indicates that, in addition to matching the plasmonic resonant wavelength of the metal and dielectric materials, an optimized

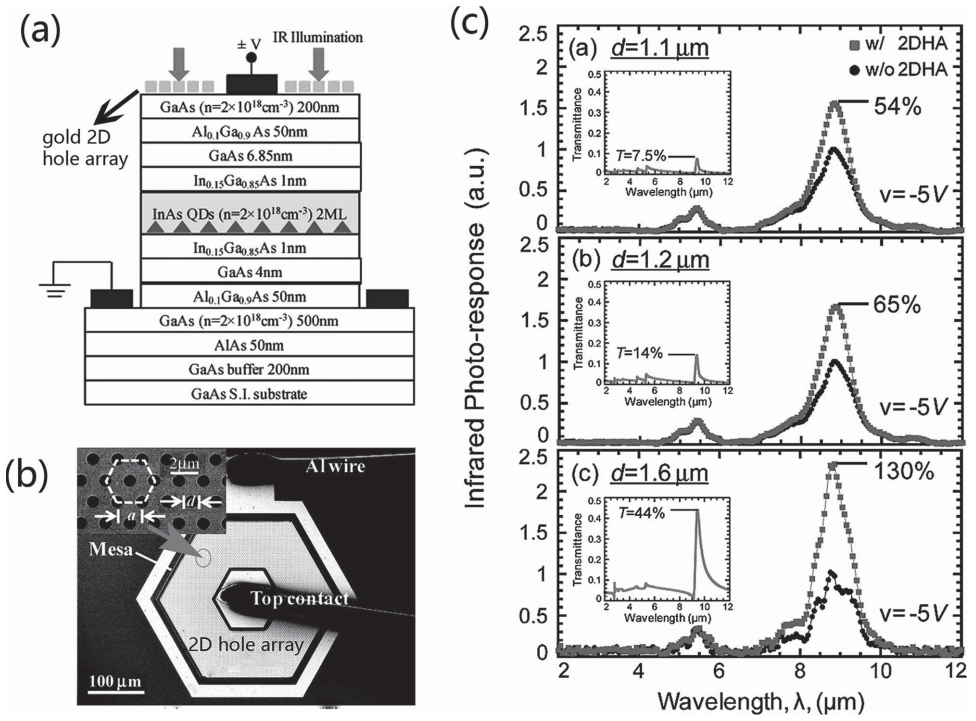

Figure 17. Single-band enhanced plasmonic photodetection. a) A schematic of 2DHA–QD infrared detector. b) SEM image of the fabricated 2DHA–QD IP device. Insert: Higher-magnification SEM image of the 2DHA. The "*d*" is the diameter of the holes. c) Design optimization of 2D HA to improve infrared transmission and photoresponse. Inserts: transmission spectra of the 2DHA structures. Reproduced with permission.[192] Copyright 2010, American Chemical Society.

structure permitting an efficient coupling of light from the far-field to a localized plasmonic mode and a close spatial matching of the active layers are principal element for realization of surface-plasmon-enhanced photodetectors with high performance.

In addition to single-band enhancement of photodetectors with high detectivity and responsivity, surface-plasmon-resonance-enhanced multicolor photodetection, by changing some of the parameters of metallic nanostructures, have gained much attention recently.[193–195] It is easy to realize photodetection at any of the desired energies between the Schottky barrier and the bandgap of semiconductor by the plasmon-induced hot-electron photocurrent,[185,194] as well as wavelength-selective photodetection of the gapless graphene-based devices.[189,196]

As an example, integrating graphene with size-tunable Au nanostructures is a new approach to making graphene-based photodetectors achieve highly sensitive and multicolor optional photodetection.[196] As shown in **Figure 18**a, devices coupled with 50 nm wide and 30 nm high periodical nanoparticles demonstrate an enhancement peak roughly at 550 nm and a largest photocurrent response to a yellow–green color. When increasing the size of the nanoparticles to 100 nm, the device yielded a photocurrent enhancement peak corresponding to yellow color detection. Larger gold nanoparticles array result in even more of a red shift of the photocurrent response peak to more than 633 nm and a frequency-selective detection of the infrared light. Therefore, the discovery in this work provides us an additional possible way to fabricate graphene-based photodetectors with multicolor photosensor pixels integrated in small packaging for high-performance-imaging optical communication.

Besides the graphene-based photodetectors described above, photodetectors with the metallic gating patterned on the silicon substrate have also realized a tunable enhacement of the photodetection in the infrared region.[194] Importantly, the response frequencies are mainly determined by the sizes of the metallic periodically spaced slits and limited by the Schottky barrier, rather than the bandgap of silicon. As shown in the inset of Figure 18b, the fabricated devices consisted of high-purity Au gratings with different grating periods on an n-type silicon wafer with a 2-nm-thick titanium adhesion layer. The responsivity peaks exhibit a linear red-shift with increasing interslit distance (*D*) of the gold gate from 1295 nm to 1635 nm (Figure 18b). The authors demonstrated that this linearity is mainly caused by the surface charge distribution or mode number on the Au grating. There is no doubt that this design concept will open up the possibility of fabricating plasmonic sensors with direct electrical readout by using these linear tunable wavelength-selective photodetectors. Hence, surface plasmons are indeed a fascinating technique for fabricating photodetectors with a high response. Moreover, there is plenty of room to further explore the advantages of plasmonic photodetectors, such as higher integration densities without consideration of the subwavelength diffraction limit, higher-band-width operation by the plasmon-assisted fast

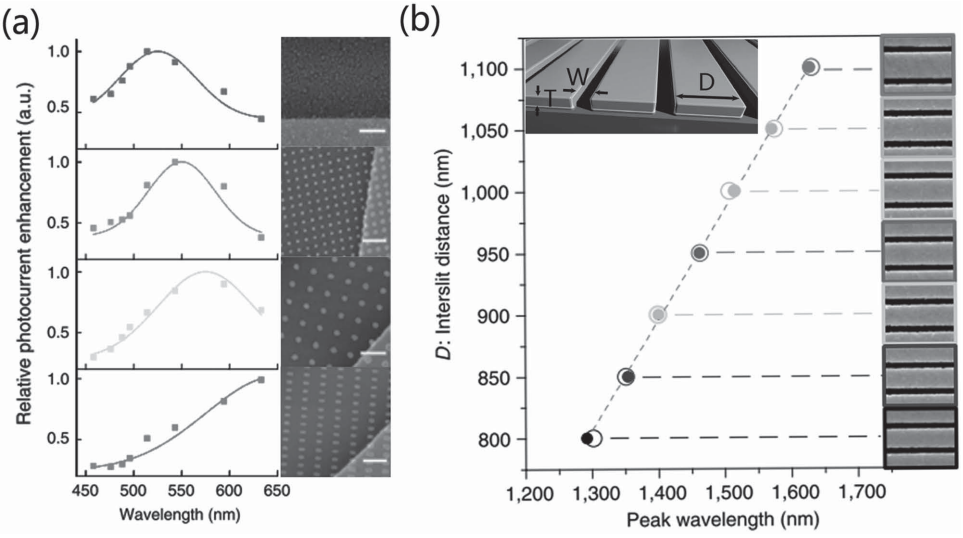

Figure 18. Multiband enhanced plasmonic photodetection by varying the parameters of metallic patterns. a) Photoresponse of several nanoparticle patterns. The plots on the left side are the photoresponse dependence of wavelength and those on the right side are SEM images of the nanoparticle patterns. Scale bar is 400 nm. b) FDTD (empty circles) and experimental data (filled circles) for the responsivity peak position in wavelength showing a linear dependence on gate distance (grey dashed line). The images on the right show a representative top-view SEM image of the grating for each corresponding responsivity peak. Inset: Schematic of a gold grating on an n-type silicon substrate, with D, W and T labeled. Reproduced with permission.[194] Copyright 2011 Macmillan Publishers Limited. b) Reproduced with permission.[196] Copyright 2013, Macmillan Publishers Limited.

transition, and reduced operation energy owing to enhanced light–matter interactions, etc.[197]

3.1.2. High-Performance Optical-Fiber Photodetectors Arising from the Pizeo-phototronic Effect

In addition to the well-known surface plasmon effect mentioned above, fabricating photodetectors by using the piezo-phototronic effect is an alternative avenue to enhance photoresponsivity. The piezo-phototronic effect is a result of three-way coupling of piezoelectric polarization, semiconductor, and photon excitation in piezoelectric semiconductors, which was proposed by Wang in 2010.[198,199] The piezo-phototronic effect in photodetectors is equivalent to applying an additional bias voltage by a strain-induced piezo-potential, just like the "gate" in a phototransistor tunes/controls the charge-transport behavior. A typical example of piezo-phototronic UV–vis photodetectors based on an optical-fiber–nanowire hybridized structures is shown on the right of **Figure 19**a.[200] It adopted a ZnO/CdS nanowire heterojunction as the active materials of the devices, which are synthesized coaxially around an optical fiber (OF). The special OF architecture allows axial illumination with light propagating inside the OF with low energy losses. The influence of strain on the device in the dark and under the off-axial illumination is shown in Figure 19b–d. Obviously, the current is increasing along with the strain under 2 bias voltage without any illumination (Figure 19b), which demonstrates that an additional bias voltage could be generated by a strain-induced piezopotential. In the following, the relative changes of photoresponsivity (R) as $\Delta R/R_0$ (R_0 is the corresponding R under strain-free conditions) at different power density were characterized. It can be found in Figure 19c, $\Delta R/R_0$ increases along with the power of the incident light as well as applied external strain, and the largest relative change of R of 820% was obtained at –1.06% strain and a power density of 1.5×10^{-3} W cm^{-2}. The aforementioned enhancement of photoresponsivity can be understood from the band diagram (Figure 19d). When a reverse bias is applied to the strain-free nanowire, an energy barrier is formed at the ZnO/CdS heterojunction interface due to the upward shift of the ZnO conduction band (Figure 19d, upper). If an external strain were applied, the heterojunction interface would suffer from positive piezo-polarization charges, which effectively reduces the barrier height by lowering both the conduction and valence band of the ZnO nanowire (Figure 19d, lower). Therefore, the electronic-transport process is significantly facilitated due to the reduced barrier height. Therefore, thanks to the piezo-phototronic effect, the properties of the photodetectors are impressive and competitive with other reported nanostructure-based visible detectors.

3.2. Special and Multifunctional Photodetectors Based on the Hybrid Nano-Building Block

In addition to improving the performance of photodetectors following the "5S" criteria, researchers have also explored many new hybrid building blocks with a wealth of physical properties. For instance, taking advantage of metallic and superconducting interfaces between insulating oxides has led to rewritable nanoscale photodetectors. A multifunctional programmable memory device is generated by gate-tuneable persistent photoconductivity. Moreover, combining the electronic properties of hybrid heterostructures offers the possibility of

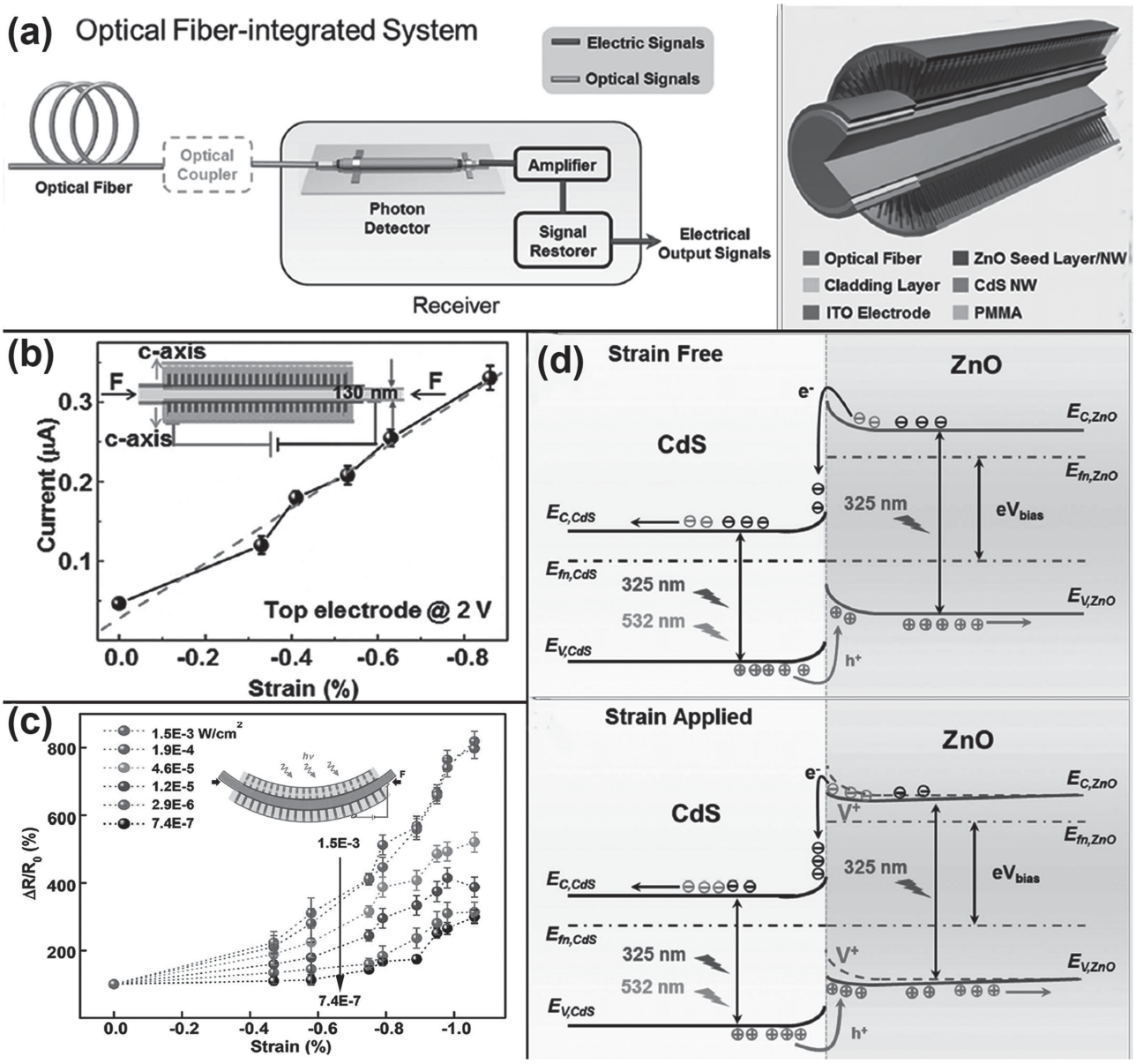

Figure 19. Piezo-phototronic UV–visible photosensing with optical-fiber–nanowire hybridized structures. a) Schematic illustration of direct integration in an optical communications system in a coupler-free manner (left), and the schematic demonstration of the structure of an optical fiber–nanowire hybridized UV/visible photodetector (right). b) A schematic experimental set-up and an strain curve when the top-electrode bias voltage is 2V. c) Relative changes of photoresponsivity (*R*) of an OF–nanowire hybridized UV PD operating in off-axial illumination mode under a series of power-density and external strain conditions, for a top electrode bias voltage of 2 V. The inset shows a corresponding schematic experiment set-up. d) Schematic band diagrams of ZnO/CdS heterojunctions without (upper) and with external strain (lower) applied to illustrate the working mechanism of OF–nanowire hybridized dual-mode photodetectors. Reproduced with permission.[200] Copyright 2015, Wiley-VCH.

creating photodetectors that can function as gas sensors, and optical logic gates, and so on. Hence, we will highlight these multifunctional photodetectors in this section.

3.2.1. Rewritable Nanoscale Photodetectors Based on Special Nanowire Junctions

Nanowires are usually directly fabricated by chemical vapor deposition (CVD), hydrothermal methods, or by further processing a solid thin film by the focused-ion-beam (FIB), or EBL techniques. Interestingly, using the reversible conductive atomic force microscopy (c-AFM) writing technique, Irvin et al. explored a kind of rewritable nanowire. Moreover, a rewritable nanoscale photodetector was created based on the special nanowire junctions at the interface between $LaAlO_3$ and $SrTiO_3$.[22] The rewritable characteristics are demonstrated in **Figure 20**a. First, when a positive voltage is applied on the c-AFM tip, conducting nanowires can be created/written between the source and drain electrodes. Then, if the tip voltage is changed to negative, nanowire junctions (insulating gaps)

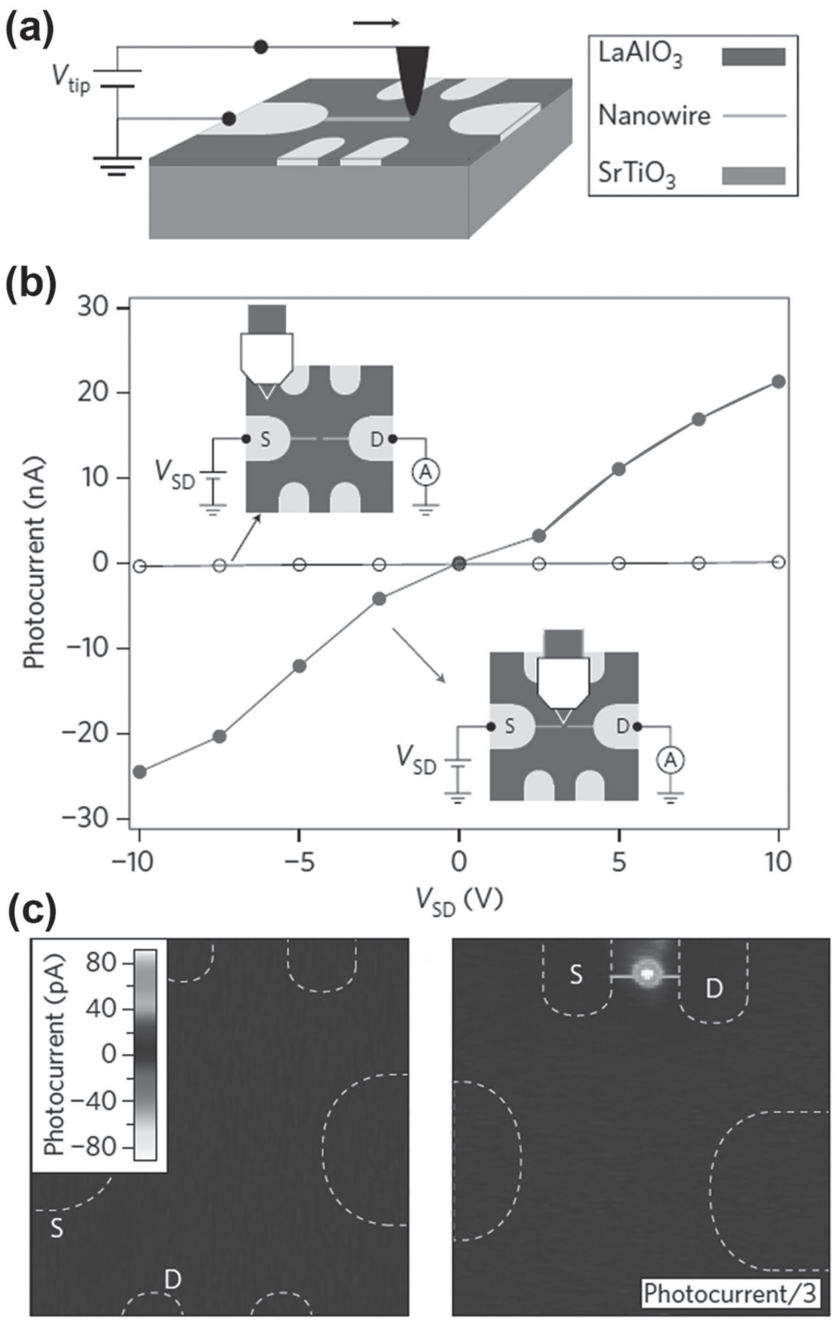

Figure 20. Rewriteable visible to near-infrared photodetector. a) Schematic illustrating how a c-AFM tip writes a nanowire at the interface between $LaAlO_3$ and $SrTiO_3$. b) Photocurrent collected from a drain electrode (D) versus source bias (V_{SD} applied to a source electrode (S)) when the laser is focused on the photodetector (closed symbols) and 25 mm away (open symbols). c) SPCM images of an area before any nanostructures are written (left), and a nanowire written close to a pair of electrodes (right). Images are 50 μm × 50 μm. Reproduced with permission.[22] Copyright 2013, Nature Publishing Group.

with an extreme nanoscale precision of 2–3 nm can be created by "cutting" these nanowires. The negative voltage here can locally restore the interface to the insulating state; thus, the nanowire is erased. The photoresponse character of a typical device is presented in Figure 20b. When the incident laser is focused far away from the gap, there is almost no current, while when the laser is spatially localized near the gap regions, a sharp increase in the photocurrent is observed. This photosensitivity is further demonstrated by the scanning photocurrent microscopy (SPCM) measurements shown in Figure 20c; when there is no nanowire device written, the SPCM image shows a spatially diffuse photocurrent of less than 2 pA (Figure 20b,c, left), but followed by writing the nanowire, the SPCM image shows a localized photocurrent in the region of the junction (Figure 20b,c, right). These electronic nanostructures can be created and erased with a high degree of precision and they are able to be relocated and reconfigured. Thus, these devices can be erased and possess the feature of rewritability.

The characteristic of writability and erasability comes from the controllability of the metal–insulator transition between the $LaAlO_3$ and $SrTiO_3$ interface. This interface undergoes an abrupt insulator-to-metal transition when the number of $LaAlO_3$ layers decreases to a critical point, and the conductance can be controlled by applying an electric field locally using the c-AFM probe.[201–203] In addition, the photoconductive response is also electric-field-tunable and spans from the visible to the near infrared regime. Since the bandgap of $SrTiO_3$ is too large to explain the visible-to-near-infrared photoresponse, the most plausible mechanism is that electrons occupying mid-gap states, which are associated with oxygen vacancies or unintentional doping, can be optically excited into the conduction band using sub-bandgap light. Therefore, the rewriteable photodetectors presented here bring new functionality to oxide nanoelectronics, which will establish a sound foundation of integrating photonic nanostructures (e.g., nanowires) with electronic components (e.g., transistors) for subwavelength optical detections.

3.2.2. Multifunctional Photoresponsive Memory Devices

As mentioned above, to enhance the properties of graphene photodetectors, several TMDC materials with strong optical absorption have been explored for integration with graphene to fabricate hybrid photodetectors with large quantum efficiency. Additionally, owing to the unique properties of these hybrid heterostructures, this offers a greater possibility of creating devices with various functionalities as well. For instance, taking advantage of carrier localization in MoS_2 and the gate-tunable persistent photoconductivity (PPC), photodetectors based

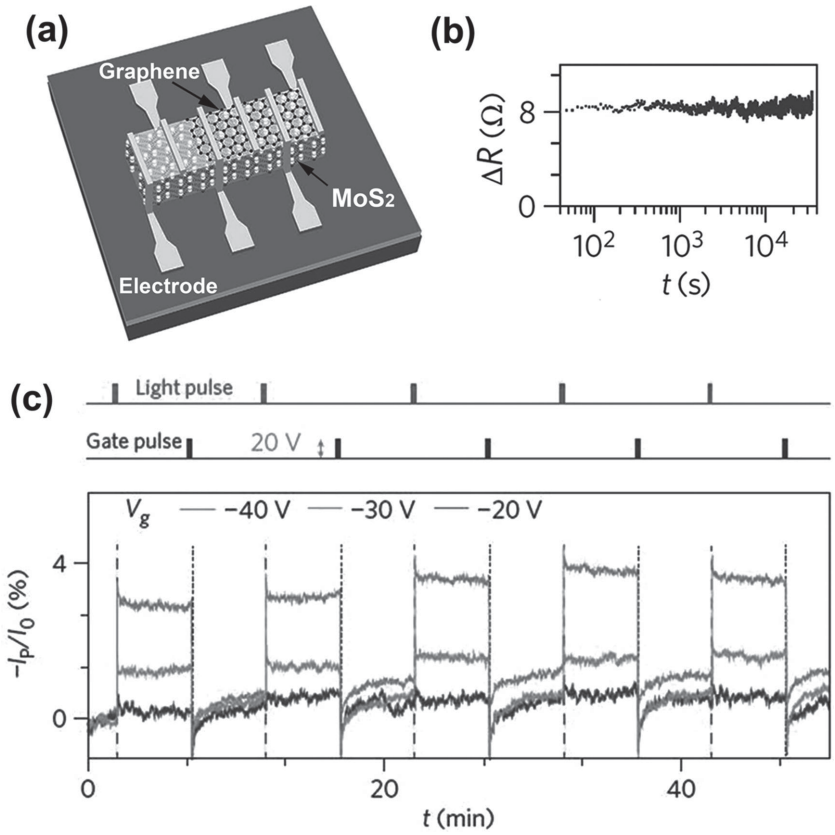

Figure 21. Graphene–MoS_2 hybrid structures for multifunctional photoresponsive memory devices. a) Schematic illustration of device architecture of a typical device. b) Persistent state over a long timescale (ca. 12 h) at a gate voltage of −40 V. c) Evolution of the switching effect as a function of V_g. For all traces, I_{LED} = 10 μA, T = 110 K. Reproduced with permission.[23] Copyright 2013, Nature Publishing Group.

on graphene–MoS_2 binary hybrid structures with additional optoelectronic functionalities involving electronic logic and memory have been explored by Roy and co-workers.[23]

As shown in **Figure 21**a, such a device is constructed by a multilayer MoS_2 flake (the thickness of the MoS_2 flake various from 2 to 10 molecular layers) overlaid with single-layer graphene (on the Si/SiO_2 substrate). It is noteworthy that, unlike the traditional heterojunction, these graphene–MoS_2 binary hybrid structures are a non-invasive physical attachment. This architecture not only preserves the high carrier mobility in graphene, but also facilitates easy exchange of the charge across the interface under the influence of an external electric field. The trap-free interface between the MoS_2 flake and the graphene gives rise to PPC, and this persistent state shows a nearly relaxation-free nature at a gate voltage of −40 V, and remains unchanged over a duration of 12 h, indicating almost perfect non-volatile charge retention (Figure 21b). Therefore, owing to the large photoconductive gain, the responsivity of the hybrids could reach up to 5×10^8 A W^{-1} at room temperature, making them the most sensitive graphene-based photodetectors. In addition, the PPC can be tuned by the gate voltage, and memory and electronic logic characteristics are demonstrated in Figure 21c. When the device is illuminated by a pulsed white LED (I_{LED} = 10 μA), the magnitude of the residual current (I_{off}) is as large as ca. 5% of the pre-illumination current (I_0) in the strongly hole-doped regime and at low temperatures. This pre-illumination state could be recovered just by a gate voltage pulse, which could elevate the Fermi energy momentarily to the conduction threshold of MoS_2 and equilibrate the charge distribution. The "light set-voltage reset" cycles could be performed over days with better than 95% accuracy in recovering the persistent state current. The above results indicate that, assisted by the graphene-on-MoS_2 stacking sequence, a new class of programmable charge-storage photodetectors with gigantic photoresponse could be realized.

3.2.3. Nanoscale Photodetectors Functioning as an "Electronic Nose"

As addressed above, nanoscale photodetectors are more and more attractive because of their compact size, as well as so many unique chemical, physical characteristics. Exceptionally, the large surface-to-volume ratio of nanostructured materials is especially facile for fabricating various gas molecules and gas sensors with high performance. For instance, high-performance few-layer GaS photodetectors with unique photoresponse in different gas environments have been reported, moreover, devices that combine photodetectors with gas sensors have been explored based on ZnO nanowires, hierarchical Bi_2S_3, CdS/ZnO core/shell nanowires, graphene, and ZnS nanowire arrays,[27,204–206] etc. Hence, all these demonstrate that these nanostructured materials are ideal building blocks for fabricating photodetectors to function as an "electronic nose". To demonstrate the photoelectric and gas-sensing characteristics of these novel multifunctional photodetectors vividly, we illustrate two typical samples of these nanodevices in the following.

As shown in **Figure 22**, Wang et al. presented a gas sensor and photodetector based on ZnS nanowires.[206] The device (Figure 22a) was fabricated by an easy and intriguing process. Simply, highly aligned nanowires arrays were obtained firstly by pressing the SiO_2/Si wafer with nanowires down on weighing paper and then pulling the weighing paper in one direction; then Ag electrodes were deposited by e-beam evaporation. Subsequently, the photosensitivity of the ZnS nanowires on a SiO_2/Si substrate was investigated. The photoresponse switching behavior of the ZnS-based photodetector demonstrated that an excellent stability (Figure 22b) and high signal-to-noise ratio (photocurrent of a few milliamperes and a low dark current at the order of nanoamperes) of the photodetector are desirable for its practical application.

Then the authors investigated the gas-sensing properties of the as-prepared ZnS-nanowire device. Firstly, it was found that 320 °C was the optimum operating temperature by changing

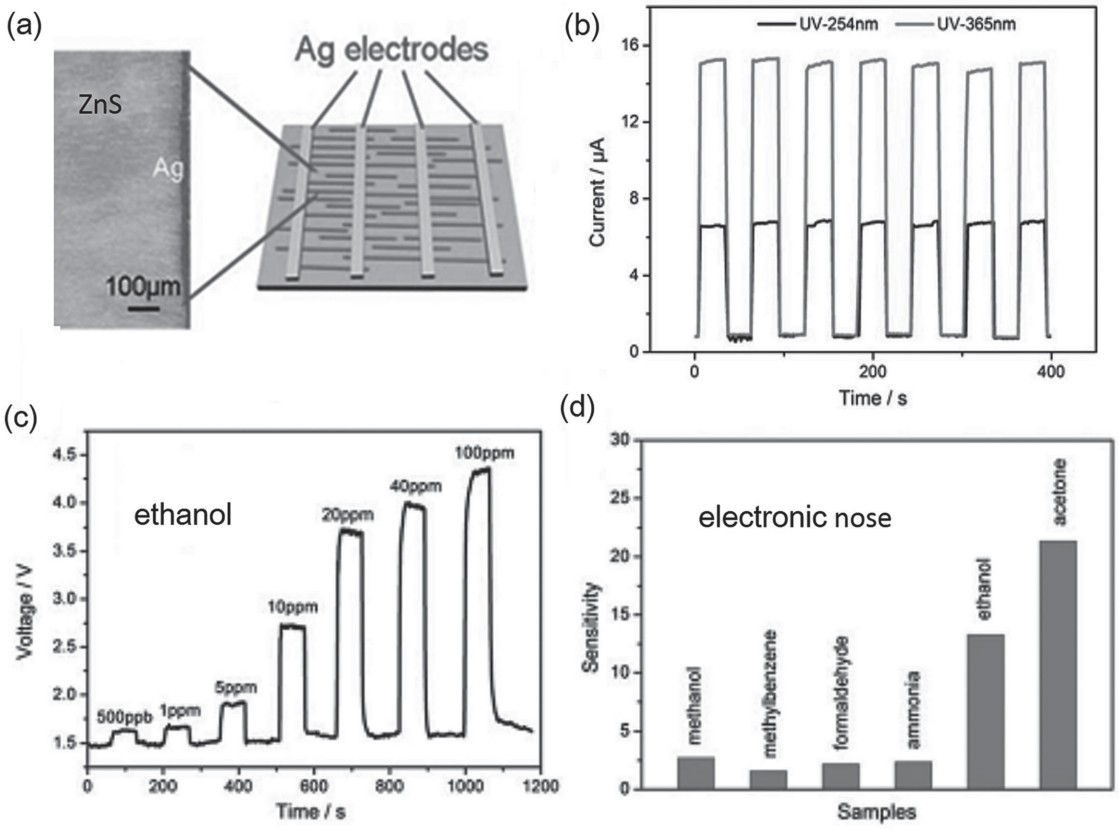

Figure 22. A gas sensor and photodetector based on ZnS nanowires. a) The photodetector based on ZnS nanowires. b) Conductance response of the device under 254 nm and 365 nm UV-light illumination for the light-on and light-off states. c) Dynamic response–recovery curves of the ethanol gas sensor toward volatile organic compounds at a series of concentrations. d) Sensing response of the gas sensors to different gases with a concentration of 100 ppm. Reproduced with permission.[206] Copyright 2012, Royal Society of Chemistry.

the operating temperature. Therefore further examination of the gas-sensing characteristics of the device was carried out at this temperature. The response to ethanol and other kinds of gases (acetone, methanol, methylbenzene, formaldehyde, and ammonia) are shown in Figure 22c,d. Both demonstrate that ZnS-nanowire-based photodetectors are indeed a promising candidate for detecting gas with high selectivity.

Aside from single 1D nanostructured materials with versatile properties, heterostructured nanowires consisting of two important functional materials are alternative building blocks for developing multifunctional photodetectors with high performance. Herein, we describe nano-photodetectors and gas sensors based on heterojunctions, which exhibit a lower hole–electron recombination rate and operating temperature, higher photocurrent and sensitivity, and better selectivity compared with nanodevices constructed from single materials. A schematic diagram of CdS/ZnO core/shell-nanowire multifunctional photodetectors presented by Yang et al.[27] is shown in **Figure 23**a. From the *I–V* characteristics and the photosensitivities of the photodetector measured under different conditions (Figure 23b,c), it can be found that the photoresponse to 367 nm light illumination is higher than that at 468 nm in these CdS/ZnO core/shell nanowires, and the photocurrent of the photodetector based on the CdS/ZnO core/shell nanowires is much larger than that of photodetectors based on a mixture of ZnO and CdS nanowires (Figure 23d). This is ascribed to the additional photoinduced electrons and effective inhibition of the recombination of photogenerated carriers in the core/shell heterojunction structure. To evaluate the advantageous gas-sensing properties of the multifunctional photodetector, the response of NO_2 gas under 468 nm light illumination of sensors based on CdS/ZnO core/shell-nanowires and a mixture of CdS and ZnO nanowires were investigated. One can see that the sensor based on the CdS/ZnO core/shell nanowires exhibits excellent gas-sensing properties, where the resistance could be changed quickly with the concentration of NO_2 gas (Figure 23e). It can also be found that the photoresponse of the present photodetector based on the CdS/ZnO core/shell nanowires is much better than that of the photodetector based on the CdS and ZnO nanowire mixture (Figure 23f). All these experimental results indicated the superiority of the core/shell structure in photodetection, as well as the optoelectronic sensing of hazardous gases.

3.2.4. Photodetectors as a Key Element of Optical Logic Gates

Similar to the transistors in logic integrated circuits,[207] photodetectors with the ability to transform light into electrical signals can also function as a key element of optical logic gates.

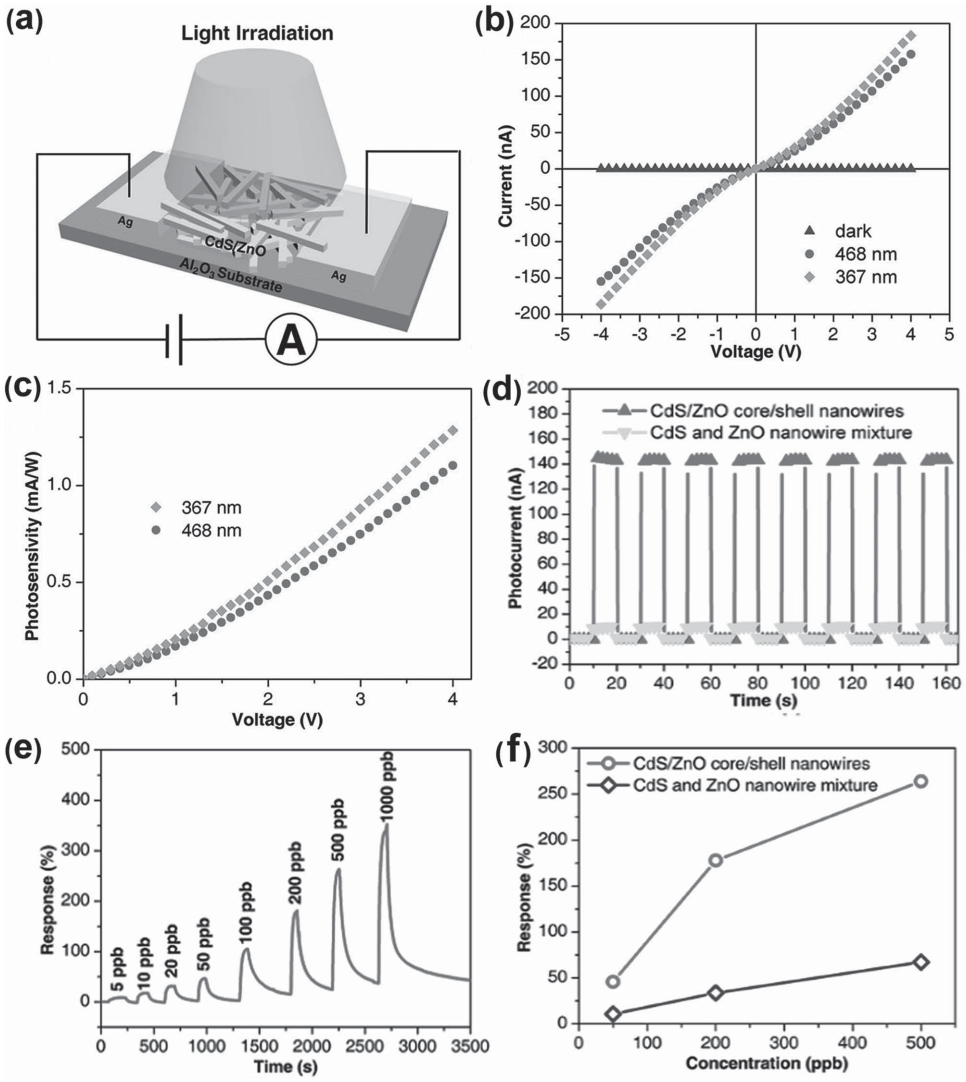

Figure 23. Multifunctional photodetectors based on CdS/ZnO core/shell nanowires. a) Schematic diagram of a photodetector constructed from CdS/ZnO core/shell nanowires. b) *I–V* characteristics of CdS/ZnO core/shell nanowire-based photodetector in the dark and illuminated with 367 nm (0.68 mW cm^{-2}), 468 nm monochromatic light (0.68 mW cm^{-2}). c) Photosensitivity calculated according to the *I–V* characteristics of the photodetector illuminated at 367 and 468 nm. d) Time-dependent photoresponse of the photodetectors based on CdS/ZnO core/shell nanowires and the mixture of CdS and ZnO nanowire mixtures measured by periodically turning on and off a 468 nm light (0.68 mW cm^{-2}) at a bias of 4 V. e) Plot of response versus time for a sensor based on CdS/ZnO core/shell nanowires upon exposure to NO_2 gas with concentrations ranging from 5 to 1000 ppb at room temperature (under illumination of 468 nm monochromatic light, 0.68 mW cm^{-2}). f) Comparison of normalized response versus NO_2 concentration of the sensors based on CdS/ZnO core/shell nanowires and the mixture of CdS and ZnO nanowires. Reproduced with permission.[27] Copyright 2014, Wiley-VCH.

To realize the similar "AND", "OR", and "NOT" logic functions, the illumination serves as the input, and the response of the photodetector in terms of photocurrent or photovoltage can be modulated to function as an electrical output with desired electrical circuit. Thus, exploring novel logic gates taking advantage of various functional photodetectors is attracting more and more attention.

As depicted in **Figure 24**a, the configuration of the integrated circuit is an optical "AND" logic gate that is constructed by combining a ZnO/GaN p–n junction UV detector with a CdSe nanowire detector.[28] As shown in Figure 24b, the ZnO/GaN junction exhibits obvious rectification characteristics under dark conditions (square data points). In addition, it had excellent photovoltaic properties under the excitation by a 325 nm He–Cd laser (380 μW $μm^{-2}$): the short-circuit current could reach about 2 μA, while the dark current is below 1 pA at zero-voltage bias, indicating the device is a self-powered UV detector with an on–off ratio larger than 10^6. Therefore, integrating the ZnO/GaN junction with a CdSe (bandgap: ca. 1.75 eV) nanowire photoconductor, a selective multi-wavelength photodetector, as well as a typical optical logic gate can be achieved. As shown in Figure 24c, only when both the CdSe-nanowire photoconductor and the ZnO/GaN junction are illuminated, the photocurrent of this hybrid system could reach a high value (1.5 nA); otherwise, when either irradiation (UV light incident on the ZnO/GaN junction or red light on the CdSe nanowire device) is tuned off, the

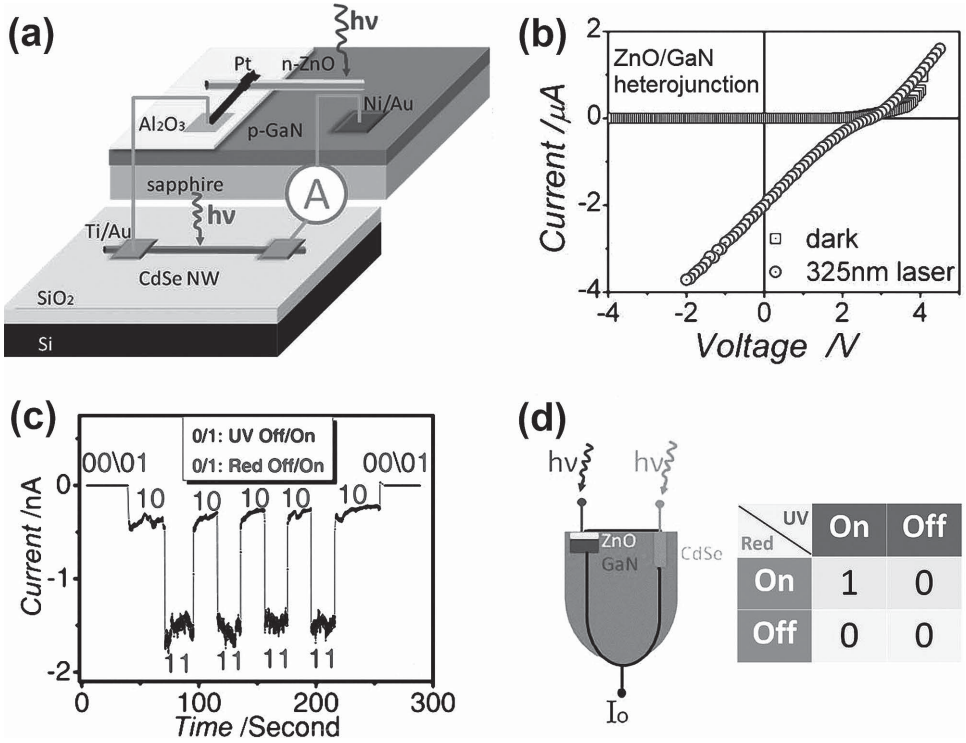

Figure 24. Optical AND logic gate constructed by combining a ZnO/GaN p–n junction UV detector with a CdSe nanowire detector. a) Schematic picture of the integrated photodetectors. b) *I–V* curves of the ZnO/GaN heterojunction in the dark (square plot) and under UV irradiation (circular plot). c) Current–time curve of the CdSe-nanowire device powered by the ZnO/GaN p–n junction with varying illumination conditions (UV and red light were incident on the heterojunction and the CdSe nanowire respectively). d) Left: the schematics of the optical AND Gate. Right: the truth table for the AND Gate. Reproduced with permission.[28] Copyright 2011, Wiley-VCH.

electrical output is at a low level (picoamperes). It is noteworthy that the relationship between the on/off light and the output photocurrent of the multi-wavelength photodetector allows it to work as an "AND" photoelectronic logic gate. To demonstrate this vividly, its schematic diagram and truth table are shown in Figure 24d. As a matter of fact, taking Figure 24a and Figure 24c together, it is easy to discover the physical mechanism behind this fascinating photoelectronic gate. In essence, it is series circuit consisting of a photovoltaic photodetector and a photoconductive photodetector. Therefore, inspired by this work, the ability to integrate present photodetectors will offer additional opportunities to create devices with various functionalities.

In addition to the "AND" gate mentioned above, Wang et al. proposed another structured optical logic gate that is based on a symmetrical Ag–nonpolar *a*-axial GaN nanowire–Ag Schottky barrier UV detector.[208] The as-prepared photodetector possessed a superhigh sensitivity up to 10^4 A W^{-1} and a fast response time less than 26 ms, which made it suitable for converting optical signals to electrical signals in real time. Then, two GaN-nanowire photodetectors were assembled in series and in parallel as an optical "AND" and "OR" gate, respectively. In addition, a kind of "NOT" gate (optical inverter) constructed via two complementary photoconductors based on porphyrin-coated silicon nanowires (SiNWs)[209] was proposed by Choi et al. The inverter was available by assembling a porphyrin-coated n-SiNW and p-SiNW in series, with one end of the n-SiNW in contact with the power supply and one end of the p-SiNW grounded. The input was illumination of white light and the output was the voltage value at the connection of the n-SiNW and p-SiNW. The photoconductance of the porphyrin-coated SiNWs was controlled by the photoinduced charge transfer from a porphyrin bound to the surface of a SiNW, which resulted in a decrease in conductance of n-SiNW, while an increase in p-SiNW when under illumination. In this work, the n- and p-SiNWs were doped at relatively high and low concentrations, respectively, which resulted in more than 1000 times higher conductance for n-SiNWs than p-SiNWs in the dark condition (the optical input was 0), so the output was a high voltage (the electrical output was 1). When under white light (optical input was 1), the photoconductance decreased for n-SiNWs and increased for p-SiNWs, leading to a low output voltage (electrical output was 0). Therefore, an excellent optical inverter ("NOT" gate) was realized.

Although logic gates based on nanostructured materials have demonstrated outstanding performance, including ZnO,[210,211] CdS,[212,213] Si[214] and MoS_2,[215] only a few reports have focused on optical logic gates.[28–209] Nanoscale optical logic gates are promising to play an important role in the integration of nanophotonics and electronics, which may have a wide range of applications including communication, interconnections, and computing, to novel diagnostics.[209] Photodetectors, especially those with a fast response and high on–off ratio, are natural candidates for optical logic gates. As reviewed above, the configurations and working principles of optical logic gates using photodetectors based on nanostructured materials as the core component can be quite different, which ensures the flexibility

Table 2. Recent progress in some nanostructured photodetectors in the last five years.

Band	Device structure	Fabrication method	Dark current	Detectivity: D^* [cm $Hz^{1/2}$ W^{-1}]	Responsivity	EQE/Gain	Response time	Year	Ref.
UV	Nb_2O_5 nanobelt	Hydrothermal and proton exchange	10.6 pA/1 V	–	15.2 A W^{-1} (1 V, 320 nm; 0.91 mW cm^{-2})	6070%	–	2011	[131]
	ZnS/ZnO nanobelt	Thermal evaporation	3.3 μA/5 V	–	5.0×10^5 A W^{-1} (5 V, 320 nm; 0.91 mW cm^{-2})	7.4×10^8% (at 5.0 V)	1.5s	2012	[137]
	K_2NbO_{21} nanowires	A facile molten method	1.2 pA/5 V	–	2.53 A W^{-1} (5 V, 320 nm; 0.12 mW cm^{-2})	9.82	<0.3s	2014	[128]
	AlN micro-/nanowire	PVT	<100 Fa/20 V	–	0.39 A W^{-1} (50 V, 190 nm)	254%	<0.3s	2015	[216]
	ZnO–Ga_2O_3 core–shell microwire	CVD	0.535 nA/–6V	9.91×10^{14}	1.3×10^3 A W^{-1} (–6 V, 254 nm; 1.67 mW cm^{-2})	2.5×10^6%	815 μs	2015	[34]
	SnO_2 microrod	CVD	13 μA/1 V	1.5×10^9	3×10^8 A W^{-1} (2 V, 250 nm; 0.03 μW cm^{-2})	1.5×10^9	<1s	2015	[184]
Visible	V_2O_5 nanowire resistor	Hydrothermal method	12.5 nA/1 V	–	482 A W^{-1} (1 V, 450 nm; 2.8 mW cm^{-2})	1328	–	2010	[53]
	CdSe nanobelt based MESFET	CVD	–	–	1400 A W^{-1} ($V_{GS} = -1$ V, $V_{DS} = 1$ V, 633 nm; 300 mW cm^{-1})	2700	35/60 s	2012	[64]
	ZnTe/CdSe NR heterojunction diode	Co-thermal evaporation method	1.3 nA/–2 V	–	39 A W^{-1} (–2 V, white light; 0.35 mW cm^{-2})	102.9	37/118 s	2014	[141]
	Biaxial CdS/CdSe/CdS nanobelt resistor	Thermal evaporation method	0.07 pA/5 V	–	642 A W^{-1} (5V, 500 nm; 2.81 mW cm^{-2})	2560	–	2015	[138]
	SiNW array/CQD core–shell heterojunction	Chemical etching and electrochemical etching method	–	3.79×10^9	0.353 A W^{-1} (0 V, 600 nm; 100 mW cm^{-2})	0.693	20/40 s	2014	[217]
Broad-band IR	Monolayer graphene quantum dots	Micromechanical exfoliation and etching	–	1.8×10^{-15} at $V_{ds} = 8$ V and $V_{gate} = -70$ V	8.61 A W^{-1} (0.1 V, 532 nm)	–	Tens of seconds	2013	[96]
	MoS_2	Micromechanical cleavage	–	–	880 A W^{-1} (0.1 V, 561 nm; ca. 2.38 mW cm^{-2})	–	4s/9s at $V_{ds} = 8$ V and $V_{gate} = -70$ V	2013	[108]
	Few-layered InSe	Mechanically exfoliated	–	2.26×10^{12}	12.3 A W^{-1} ($V_g = 0$, $V_{ds} = 10$ V, 450 nm) 157 A W^{-1} ($V_g = 10$, $V_{ds} = 70$ V, 633 nm)	3389% at 450 nm 30755% at 633 nm	ca. 50 ms	2014	[103]
	In_2Se_3 nanosheets	Micromechanical exfoliation	–	–	395 A W^{-1} (5 V, 300 nm)	1.63×10^5%	180 ms	2014	[106]
	GaTe	Mechanically exfoliated	–	10^{12}–10^{13}	10^4 A W^{-1} (5 V, 532 nm; <30 nW cm^{-2})	–	6 ms	2014	[65]
	GaS	Mechanical cleavage	–	2.1×10^{11} J	19.2 A W^{-1} (2V, 254 nm)	9371%	<30 ms	2013	[104]
	Bi_2S_3	Solvothermal process	–	–	4.4 A W^{-1} (0.5 V, 632.8 nm, 1.6 mW cm^{-2})	860%	ca. 10/350 μs	2015	[218]

Table 2. Continued.

Band	Device structure	Fabrication method	Dark current	Detectivity: D^* [cm $Hz^{1/2}$ W^{-1}]	Responsivity	EQE/Gain	Response time	Year	Ref.
THz	Graphene	Mechanical exfoliation	30 nA	–	100 mV W^{-1} (2V, THz)	–	–	2012	[219]
	p–n junction film of aligned carbon nanotubes	Chemical vapor deposition	20 nA	–	2.5 V W^{-1} (1 mV, 3.11 THz, ca. 150 mW, 2.4 V W^{-1} (1 mV, 2.52 THz, ca. 150 mW) 1.7 V W^{-1} (1 mV,1.39 THz, ca. 150 mW)	–	–	2014	[143]
	PbS QDs/graphene	Mechanical exfoliation/deposition from solution	–	7×10^{13}	5×10^{7} A W^{-1} (1V, 532 nm, 1.7 pW)	–	ca. 10–20 ms	2012	[177]
	GQD	Modified mummers method	ca. 10 μA	2.4×10^{11}	0.5 A W^{-1} (5.5 V, 800 nm)	–	2–30 μs	2014	[171]

for rational design and facile fabrication processes of this kind of device. It can be inferred that optical logic gates have the potential to open up new research areas and create new possibilities for the fabrication of special functional and multifunctional photodetectors.

4. Conclusion and Outlook

As appealing platforms, nanostructured materials with a number of intriguing and excellent photoelectric properties have established themselves as versatile building blocks in terms of interconnects and functional units for novel photodetectors. Moreover, it is expected that they will play an important role in improving the performance and extending the function of traditional photodetectors. To describe the developing trend in this flourishing area vividly, examples of typical nanoscale photodetectors, covering the UV to THz frequency ranges, developed over the past 5 years are summarized herein. As shown in **Table 2**, in addition to sophisticated nanofabrication techniques such as FIB and EBL, the majority of nanostructured materials can be fabricated directly by a host of powerful low-cost approaches involving hydrothermal/solvothermal reactions, CVD, and solution-based self-assembly, etc. Benefiting from the large surface-to-volume ratios and small size comparable to the Debye length of the aforementioned materials, a variety of prototype photodetectors have been explored with excellent photoelectronic properties. A continuous progression of their performance is witnessed by improving the shape, and the geometry of the desired nanostructured materials. However, with regard to the overall perspective, the study of nanoscale photodetectors is still at its preliminary stage. To take full advantage of nanoscale materials' unique photoelectronic properties for practical applications, studies of many issues need to be urgently intensified.

In view of the basic scientific research and potential technological applications, a roadmap for further development of nanoscale photodetectors is described as follows. Firstly, the ability to control nanostructured materials precisely is essential for high-performance nanodevices. Strategies that are facile, low-cost, highly reliable, and repeatable for fabricating the versatile nanostructured materials used in nanoscale photodetectors should be developed. Secondly, research focusing on modifying the properties of existing devices by doping, surface treatment, and designing distinct functional structures (optical microcavities, photonic crystals, etc.) are needed. Thirdly, from the perspective of practical applications, developing commonly applicable methods for scaling up the yield of nanostructured materials (isolate or grow) with good alignment and uniform distribution is critical for fabricating devices with high performance. Additionally, designing a suitable architecture of novel photoelectronic components compatible with traditional photodetectors is an appalling avenue to bring the nanostructured materials out of the lab for increasing the integration of the present devices.

Although many riddles need to be solved, behind this burgeoning field, it is no doubt that the combination of well-studied materials and established device fabrication technologies will lead to more and more exciting discoveries in the further development of photodetectors. In view of the complexity of researching and developing nanoscale photodetectors, research tools from different disciplines including physics, chemistry, materials science, and microelectronics need to be pulled together to solve these problems. Of course, challenges mean opportunities as well, the entirely new era of photodetection is beckoning us on, and we do hope this review will inspire an increasing number of researchers and engineers to join this game.

Acknowledgements

H.Y.C., H.L., Z.M.Z. and K.H contributed equally to this work. This work was supported by the National Natural Science Foundation of China (Grant No. 51471051), Science and Technology Commission of Shanghai Municipality (13NM1400300), Shanghai Shu Guang Project

(12SG01), and the Programs for Professor of Special Appointment (Eastern Scholar) at Shanghai Institutions of Higher Learning.

Received: July 22, 2015
Revised: August 18, 2015
Published online: November 25, 2015

[1] G. Rieke, *Detection of Light: From the Ultraviolet to the Submillimeter*, Cambridge University Press, Cambridge, UK, **2003**.
[2] M. Geis, S. Spector, M. Grein, R. Schulein, J. Yoon, D. Lennon, S. Deneault, F. Gan, F. Kaertner, T. Lyszczarz, *IEEE Photonics Technol. Lett.* **2007**, *19*, 152.
[3] H. Elgala, R. Mesleh, H. Haas, *IEEE Commun. Mag.* **2011**, *49*, 56.
[4] A. M. Waxman, A. N. Gove, D. A. Fay, J. P. Racamato, J. E. Carrick, M. C. Seibert, E. D. Savoye, *Neural Networks* **1997**, *10*, 1.
[5] B. H. Stuart, *Infrared Spectroscopy: Fundamentals and Applications*, Analytical Techniques in the Sciences, John Wiley and Sons, Chichester, UK **2005**.
[6] R. Weissleder, C. H. Tung, U. Mahmood, A. Bogdanov, *Nat. Biotechnol.* **1999**, *17*, 375.
[7] X. Huang, I. H. El-Sayed, W. Qian, M. A. El-Sayed, *J. Am. Chem. Soc.* **2006**, *128*, 2115.
[8] D. V. Meledin, D. P. Marrone, C. Y. E. Tong, H. Gibson, R. Blundell, S. N. Paine, D. C. Papa, M. Smith, T. R. Hunter, J. Battat, B. Voronov, G. Gol'tsman, *IEEE Trans. Microwave Theory Tech.* **2004**, *52*, 2338.
[9] J. Zmuidzinas, *IEEE Photonics Conf.*, IEEE, Piscataway, NJ, USA **2012**, p. 226.
[10] L. Hou, H. Park, X. C. Zhang, *IEEE J. Sel. Top. Quantum Electron.* **2011**, *17*, 177.
[11] M. Bohr, K. Mistry, Intel 22 nm Technology, http://www.intel.com/content/www/us/en/silicon-innovations/intel-22nm-technology.html (accessed: September 2015).
[12] A. D. Franklin, M. Luisier, S. J. Han, G. Tulevski, C. M. Breslin, L. Gignac, M. S. Lundstrom, W. Haensch, *Nano Lett.* **2012**, *12*, 758.
[13] H. Iwai, *Microelectron. Eng.* **2009**, *86*, 1520.
[14] Samsung Announces Mass Production of Industry's First 14 nm FinFET Mobile Application Processor, http://www.samsung.com/global/business/semiconductor/news-events/press-releases/detail?newsId=14001 (accessed: September, 2015).
[15] IBM Research Alliance Produces Industry's First 7 nm Node Test Chips, https://www-03.ibm.com/press/us/en/pressrelease/47301.wss (accessed: September, 2015).
[16] G. Konstantatos, E. H. Sargent, *Nat. Nanotechnol.* **2010**, *5*, 391.
[17] A. Thiaville, J. Miltat, *Science*, *284*, **1999**, 1939.
[18] C. Soci, A. Zhang, X. Y. Bao, H. Kim, Y. Lo, D. Wang, *J. Nanosci. Nanotechnol.* **2010**, *10*, 1430.
[19] H. A. Atwater, A. Polman, *Nat. Mater.* **2010**, *9*, 205.
[20] J. A. Schuller, E. S. Barnard, W. Cai, Y. C. Jun, J. S. White, M. L. Brongersma, *Nat. Mater.* **2010**, *9*, 193.
[21] R. Zia, J. A. Schuller, A. Chandran, M. L. Brongersma, *Mater. Today* **2006**, *9*, 20.
[22] P. Irvin, Y. J. Ma, D. F. Bogorin, C. Cen, C. W. Bark, C. M. Folkman, C. B. Eom, J. Levy, *Nat. Photonics* **2010**, *4*, 849.
[23] K. Roy, M. Padmanabhan, S. Goswami, T. P. Sai, G. Ramalingam, S. Raghavan, A. Ghosh, *Nat. Nanotechnol.* **2013**, *8*, 826.
[24] S. P. Chang, K. Y. Chen, *ISRN Nanotechnol.* **2012**, *2012*, 1.
[25] N. Gogurla, A. K. Sinha, S. Santra, S. Manna, S. K. Ray, *Sci. Rep.* **2014**, *4*, 6483.
[26] J. Hodgkinson, R. P. Tatam, *Meas. Sci. Technol.* **2013**, *24*, 012004.
[27] Z. Yang, L. Guo, B. Zu, Y. Guo, T. Xu, X. C. Dou, *Adv. Opt. Mater.* **2014**, *2*, 738.
[28] Y. Q. Bie, Z. M. Liao, H. Z. Zhang, G. R. Li, Y. Ye, Y. B. Zhou, J. Xu, Z. X. Qin, L. Dai, D. P. Yu, *Adv. Mater.* **2011**, *23*, 649.
[29] H. Y. Chen, K. W. Liu, L. F. Hu, A. A. Al-Ghamdi, X. S. Fang, *Mater. Today* **2015**, DOI :10.1016/j.mattod.2015.06.001.
[30] K. W. Liu, M. Sakurai, M. Aono, *Sensors (Basel)* **2010**, *10*, 8604.
[31] L. Peng, L. F. Hu, X. S. Fang, *Adv. Funct. Mater.* **2014**, *24*, 2591.
[32] M. Razeghi, A. Rogalski, *J. Appl. Phys.* **1996**, *79*, 7433.
[33] F. H. L. Koppens, T. Mueller, P. Avouris, A. C. Ferrari, M. S. Vitiello, M. Polini, *Nat. Nanotechnol.* **2014**, *9*, 780.
[34] B. Zhao, F. Wang, H. Chen, Y. Wang, M. Jiang, X. S. Fang, D. X. Zhao, *Nano Lett.* **2015**, *15*, 3988.
[35] L. W. Sang, M. Y. Liao, M. Sumiya, *Sensors (Basel)* **2013**, *13*, 10482.
[36] S. M. Sze, K. K. Ng, *Physics of Semiconductor Devices*, John Wiley & Sons, Hoboken, NJ, USA **2006**.
[37] S. E. Keuleyan, P. Guyot-Sionnest, C. Delerue, G. Allan, *ACS Nano* **2014**, *8*, 8676.
[38] F. Prins, M. Buscema, J. S. Seldenthuis, S. Etaki, G. Buchs, M. Barkelid, V. Zwiller, Y. Gao, A. J. Houtepen, L. D. Siebbeles, *Nano Lett.* **2012**, *12*, 5740.
[39] L. Tang, R. Ji, X. Li, G. Bai, C. P. Liu, J. Hao, J. Lin, H. Jiang, K. S. Teng, Z. Yang, *ACS Nano* **2014**, *8*, 6312.
[40] D. Kufer, I. Nikitskiy, T. Lasanta, G. Navickaite, F. H. Koppens, G. Konstantatos, *Adv. Mater.* **2015**, *27*, 176.
[41] E. Lhuillier, S. Keuleyan, P. Zolotavin, P. Guyot-Sionnest, *Adv. Mater.* **2013**, *25*, 137.
[42] J. Schornbaum, B. Winter, S. P. Schießl, F. Gannott, G. Katsukis, D. M. Guldi, E. Spiecker, J. Zaumseil, *Adv. Funct. Mater.* **2014**, *24*, 5798.
[43] S. Strite, H. Morkoç, *J. Vac. Sci. Technol. B* **1992**, *10*, 1237.
[44] K. Takahashi, A. Yoshikawa, A. Sandhu, *Wide-Bandgap Semiconductors*, Springer, New York **2007**.
[45] R. Suzuki, S. Nakagomi, Y. Kokubun, *Appl. Phys. Lett.* **2011**, *98*, 131114.
[46] K. Liu, M. Sakurai, M. Aono, *J. Mater. Chem.* **2012**, *22*, 12882.
[47] Z. Jarzebski, J. Marton, *J. Electrochem. Soc.* **1976**, *123*, 299C.
[48] S. Silva, G. Amaratunga, E. Salje, K. Knowles, *J. Mater. Sci.* **1994**, *29*, 4962.
[49] H. Tang, K. Prasad, R. Sanjinès, P. E. Schmid, F. Lévy, *J. Appl. Phys.* **1994**, *75*, 2042.
[50] X. S. Fang, S. L. Xiong, T. Y. Zhai, Y. Bando, M. Y. Liao, U. K. Gautam, Y. Koide, X. Zhang, Y. T. Qian, D. Golberg, *Adv. Mater.* **2009**, *21*, 5016.
[51] M. Aven, B. Segall, *Phys. Rev.* **1963**, *130*, 81.
[52] K. Deng, L. Li, *Adv. Mater.* **2014**, *26*, 2619.
[53] T. Y. Zhai, H. Liu, H. Li, X. S. Fang, M. Y. Liao, L. Li, H. Zhou, Y. Koide, Y. Bando, D. Golberg, *Adv. Mater.* **2010**, *22*, 2547.
[54] T. D. Golden, M. G. Shumsky, Y. Zhou, R. A. VanderWerf, R. A. van Leeuwen, J. A. Switzer, *Chem. Mater.* **1996**, *8*, 2499.
[55] Y. S. Lee, M. T. Winkler, S. C. Siah, R. Brandt, T. Buonassisi, *Appl. Phys. Lett.* **2011**, *98*, 192115.
[56] L. F. Hu, L. M. Wu, M. Y. Liao, X. S. Fang, *Adv. Mater.* **2011**, *23*, 1988.
[57] N. Huo, S. Yang, Z. Wei, S.-S. Li, J.-B. Xia, J. Li, *Sci. Rep.* **2014**, *4*, 5209.
[58] Y. Deng, Z. Luo, N. J. Conrad, H. Liu, Y. Gong, S. Najmaei, P. M. Ajayan, J. Lou, X. Xu, P. D. Ye, *ACS Nano* **2014**, *8*, 8292.
[59] F. N. Xia, H. Wang, D. Xiao, M. Dubey, A. Ramasubramaniam, *Nat. Photonics* **2014**, *8*, 899.
[60] L. Li, Y. Yu, G. J. Ye, Q. Ge, X. Ou, H. Wu, D. Feng, X. H. Chen, Y. Zhang, *Nat. Nanotechnol.* **2014**, *9*, 372.
[61] A. Brown, S. Rundqvist, *Acta Crystallogr.* **1965**, *19*, 684.

[62] K. F. Mak, C. Lee, J. Hone, J. Shan, T. F. Heinz, *Phys. Rev. Lett.* **2010**, *105*, 136805.
[63] B. Radisavljevic, A. Radenovic, J. Brivio, V. Giacometti, A. Kis, *Nat. Nanotechnol.* **2011**, *6*, 147.
[64] Y. Dai, B. Yu, Y. Ye, P. Wu, H. Meng, L. Dai, G. Qin, *J. Mater. Chem.* **2012**, *22*, 18442.
[65] F. Liu, H. Shimotani, H. Shang, T. Kanagasekaran, V. Zolyomi, N. Drummond, V. I. Fal'ko, K. Tanigaki, *ACS Nano* **2014**, *8*, 752.
[66] W. Walukiewicz, J. Lagowski, L. Jastrzebski, P. Rava, M. Lichtensteiger, C. Gatos, H. Gatos, *J. Appl. Phys.* **1980**, *51*, 2659.
[67] J. Wang, M. S. Gudiksen, X. Duan, Y. Cui, C. M. Lieber, *Science* **2001**, *293*, 1455.
[68] M. S. Gudiksen, J. Wang, C. M. Lieber, *J. Phys. Chem. B* **2001**, *105*, 4062.
[69] G. Chen, B. Liang, X. Liu, Z. Liu, G. Yu, X. Xie, T. Luo, D. Chen, M. Zhu, G. Shen, *ACS Nano* **2013**, *8*, 787.
[70] G. Haacke, G. Castellion, *J. Appl. Phys.* **1964**, *35*, 2484.
[71] P. Stiles, E. Burstein, D. Langenberg, *J. Appl. Phys.* **1961**, *32*, 2174.
[72] H. Liu, M. Li, O. Voznyy, L. Hu, Q. Fu, D. Zhou, Z. Xia, E. H. Sargent, J. Tang, *Adv. Mater.* **2014**, *26*, 2718.
[73] C. Keffer, T. M. Hayes, A. Bienenstock, *Phys. Rev. Lett.* **1968**, *21*, 1676.
[74] J. Butler, A. Calawa, R. PhelanJr., T. Harman, A. Strauss, R. Rediker, *Appl. Phys. Lett.* **1964**, *5*, 75.
[75] S. Y. Jang, H. S. Kim, J. Park, M. Jung, J. Kim, S. H. Lee, J. W. Roh, W. Lee, *Nanotechnology* **2009**, *20*, 415204.
[76] R. Brebrick, E. Gubner, *J. Chem. Phys.* **1962**, *36*, 1283.
[77] Y. Xu, M. A. Schoonen, *Am. Mineral.* **2000**, *85*, 543.
[78] J. Wang, J. Hu, X. Sun, A. M. Agarwal, L. C. Kimerling, D. R. Lim, R. Synowicki, *J. Appl. Phys.* **2008**, *104*, 053707.
[79] I. Robel, R. Gresback, U. Kortshagen, R. D. Schaller, V. I. Klimov, *Phys. Rev. Lett.* **2009**, *102*, 177404.
[80] Y. Yasuoka, M. Wada, *Jpn. J. Appl. Phys.* **1970**, *9*, 452.
[81] R. S. Allgaier, W. W. Scanlon, *Phys. Rev.* **1958**, *111*, 1029.
[82] W. W. Scanlon, *Phys. Rev.* **1958**, *109*, 47.
[83] D. Jariwala, V. K. Sangwan, L. J. Lauhon, T. J. Marks, M. C. Hersam, *ACS Nano* **2014**, *8*, 1102.
[84] Q. H. Wang, K. Kalantar-Zadeh, A. Kis, J. N. Coleman, M. S. Strano, *Nat. Nanotechnol.* **2012**, *7*, 699.
[85] J. H. Li, L. Y. Niu, Z. J. Zheng, F. Yan, *Adv. Mater.* **2014**, *26*, 5239.
[86] S. Z. Butler, S. M. Hollen, L. Cao, Y. Cui, J. A. Gupta, H. R. Gutierrez, T. F. Heinz, S. S. Hong, J. Huang, A. F. Ismach, E. Johnston-Halperin, M. Kuno, V. V. Plashnitsa, R. D. Robinson, R. S. Ruoff, S. Salahuddin, J. Shan, L. Shi, M. G. Spencer, M. Terrones, W. Windl, J. E. Goldberger, *ACS Nano* **2013**, *7*, 2898.
[87] A. K. Geim, K. S. Novoselov, *Nat. Mater.* **2007**, *6*, 183.
[88] F. Xia, H. Yan, P. Avouris, *Proc. IEEE* **2013**, *101*, 1717.
[89] K. F. Mak, L. Ju, F. Wang, T. F. Heinz, *Solid State Commun.* **2012**, *152*, 1341.
[90] R. Nair, P. Blake, A. Grigorenko, K. Novoselov, T. Booth, T. Stauber, N. Peres, A. Geim, *Science* **2008**, *320*, 1308.
[91] X. Xu, N. M. Gabor, J. S. Alden, A. M. van der Zande, P. L. McEuen, *Nano Lett.* **2009**, *10*, 562.
[92] T. J. Echtermeyer, P. S. Nene, M. Trushin, R. V. Gorbachev, A. L. Eiden, S. Milana, Z. Sun, J. Schliemann, E. Lidorikis, K. S. Novoselov, A. C. Ferrari, *Nano Lett.* **2014**, *14*, 3733.
[93] P. Gowda, D. R. Mohapatra, A. Misra, *ACS Appl. Mater. Interfaces* **2014**, *6*, 16763.
[94] M. Freitag, T. Low, P. Avouris, *Nano Lett.* **2013**, *13*, 1644.
[95] V. Patil, A. Capone, S. Strauf, E. H. Yang, *Sci. Rep.* **2013**, *3*, 2791.
[96] Y. Z. Zhang, T. Liu, B. Meng, X. H. Li, G. Z. Liang, X. N. Hu, Q. J. Wang, *Nat. Commun.* **2013**, *4*, 1181.
[97] F. Xia, T. Mueller, Y. M. Lin, A. Valdes-Garcia, P. Avouris, *Nat. Nanotechnol.* **2009**, *4*, 839.
[98] C. H. Liu, Y. C. Chang, T. B. Norris, Z. H. Zhong, *Nat. Nanotechnol.* **2014**, *9*, 273.
[99] J. Yoon, W. Park, G. Y. Bae, Y. Kim, H. S. Jang, Y. Hyun, S. K. Lim, Y. H. Kahng, W. K. Hong, B. H. Lee, H. C. Ko, *Small* **2013**, *9*, 3295.
[100] W. Choi, M. Y. Cho, A. Konar, J. H. Lee, G.-B. Cha, S. C. Hong, S. Kim, J. Kim, D. Jena, J. Joo, S. Kim, *Adv. Mater.* **2012**, *24*, 5832.
[101] N. Perea-Lopez, A. L. Elias, A. Berkdemir, A. Castro-Beltran, H. R. Gutierrez, S. Feng, R. Lv, T. Hayashi, F. Lopez-Urias, S. Ghosh, B. Muchharla, S. Talapatra, H. Terrones, M. Terrones, *Adv. Funct. Mater.* **2013**, *23*, 5511.
[102] J. S. Ross, P. Klement, A. M. Jones, N. J. Ghimire, J. Yan, D. G. Mandrus, T. Taniguchi, K. Watanabe, K. Kitamura, W. Yao, D. H. Cobden, X. Xu, *Nat. Nanotechnol.* **2014**, *9*, 268.
[103] S. R. Tamalampudi, Y. Y. Lu, U. R. Kumar, R. Sankar, C. D. Liao, B. K. Moorthy, C. H. Cheng, F. C. Chou, Y. T. Chen, *Nano Lett.* **2014**, *14*, 2800.
[104] P. Hu, L. Wang, M. Yoon, J. Zhang, W. Feng, X. Wang, Z. Wen, J. C. Idrobo, Y. Miyamoto, D. B. Geohegan, K. Xiao, *Nano Lett.* **2013**, *13*, 1649.
[105] P. Hu, Z. Wen, L. Wang, P. Tan, K. Xiao, *ACS Nano* **2012**, *6*, 5988.
[106] R. B. Jacobs-Gedrim, M. Shanmugam, N. Jain, C. A. Durcan, M. T. Murphy, T. M. Murray, R. J. Matyi, R. L. Moore, B. Yu, *ACS Nano* **2014**, *8*, 514.
[107] A. Ramasubramaniam, D. Naveh, E. Towe, *Phys. Rev. B* **2011**, *84*, 205325.
[108] O. Lopez-Sanchez, D. Lembke, M. Kayci, A. Radenovic, A. Kis, *Nat. Nanotechnol.* **2013**, *8*, 497.
[109] R. F. Service, *Science* **2015**, *348*, 490.
[110] M. Buscema, D. J. Groenendijk, S. I. Blanter, G. A. Steele, H. S. J. van der Zant, A. Castellanos-Gomez, *Nano Lett.* **2014**, *14*, 3347.
[111] M. Engel, M. Steiner, P. Avouris, *Nano Lett.* **2014**, *14*, 6414.
[112] N. Youngblood, C. Chen, S. J. Koester, M. Li, *Nat. Photonics* **2015**, DOI: 10.1038/nphoton.2015.23.
[113] H. Yuan, X. Liu, F. Afshinmanesh, W. Li, G. Xu, J. Sun, B. Lian, A. G. Curto, G. Ye, Y. Hikita, Z. Shen, S. Zhang, X. Chen, M. Brongersma, H. Y. Hwang, Y. Cui, *Nat. Nanotechnol.* **2015**, *10*, 707.
[114] H. Kroemer, *Rev. Mod. Phys.* **2001**, *73*, 783.
[115] D. Jariwala, V. K. Sangwan, C. C. Wu, P. L. Prabhumirashi, M. L. Geier, T. J. Marks, L. J. Lauhon, M. C. Hersam, *Proc. Natl. Acad. Sci. USA* **2013**, *110*, 18076.
[116] X. Wang, W. Tian, M. Liao, Y. Bando, D. Golberg, *Chem. Soc. Rev.* **2014**, *43*, 1400.
[117] J. N. Coleman, M. Lotya, A. O'Neill, S. D. Bergin, P. J. King, U. Khan, K. Young, A. Gaucher, S. De, R. J. Smith, *Science* **2011**, *331*, 568.
[118] K. Liu, N. Zhao, E. Kumacheva, *Chem. Soc. Rev.* **2011**, *40*, 656.
[119] Y. Zhao, L. F. Hu, H. Liu, M. Liao, X. S. Fang, L. M. Wu, *Sci. Rep.* **2014**, *4*, 6847.
[120] M. Chen, L. F. Hu, J. Xu, M. Y. Liao, L. M. Wu, X. S. Fang, *Small* **2011**, *7*, 2449.
[121] H. Chen, L. F. Hu, X. S. Fang, L. Wu, *Adv. Funct. Mater.* **2012**, *22*, 1229.
[122] L. F. Hu, M. Chen, W. Shan, T. Zhan, M. Y. Liao, X. S. Fang, X. H. Hu, L. M. Wu, *Adv. Mater.* **2012**, *24*, 5872.
[123] L. F. Hu, M. Chen, X. S. Fang, L. M. Wu, *Chem. Soc. Rev.* **2012**, *41*, 1350.
[124] S. Iijima, *Nature* **1991**, *354*, 56.
[125] Z. W. Pan, Z. R. Dai, Z. L. Wang, *Science* **2001**, *291*, 1947.

[126] T. Y. Zhai, L. Li, X. Wang, X. S. Fang, Y. Bando, D. Golberg, *Adv. Funct. Mater.* **2010**, *20*, 4233.
[127] X. S. Fang, Y. Bando, M. Y. Liao, U. K. Gautam, C. Y. Zhi, B. Dierre, B. D. Liu, T. Y. Zhai, T. Sekiguchi, Y. Koide, *Adv. Mater.* **2009**, *21*, 2034.
[128] H. Liu, Z. M. Zhang, L. F. Hu, N. Gao, L. W. Sang, M. Y. Liao, R. Z. Ma, F. F. Xu, X. S. Fang, *Adv. Opt. Mater.* **2014**, *2*, 771.
[129] P. Ren, W. Hu, Q. Zhang, X. Zhu, X. Zhuang, L. Ma, X. Fan, H. Zhou, L. Liao, X. Duan, A. L. Pan, *Adv. Mater.* **2014**, *26*, 7444.
[130] Z. Wang, M. Safdar, C. Jiang, J. He, *Nano. Lett.* **2012**, *12*, 4715.
[131] X. S. Fang, L. F. Hu, K. F. Huo, B. Gao, L. J. Zhao, M. Y. Liao, P. K. Chu, Y. Bando, D. Golberg, *Adv. Funct. Mater.* **2011**, *21*, 3907.
[132] J. Miao, W. Hu, N. Guo, Z. Lu, X. Zou, L. Liao, S. Shi, P. Chen, Z. Fan, J. C. Ho, *ACS Nano* **2014**, *8*, 3628.
[133] L. F. Hu, J. Yan, M. Y. Liao, L. M. Wu, X. S. Fang, *Small* **2011**, *7*, 1012.
[134] X. Dai, S. Zhang, Z. Wang, G. Adamo, H. Liu, Y. Huang, C. Couteau, C. Soci, *Nano Lett.* **2014**, *14*, 2688.
[135] C. Y. Hsu, D. H. Lien, S. Y. Lu, C.-Y. Chen, C. F. Kang, Y. L. Chueh, W.-K. Hsu, J. H. He, *ACS Nano* **2012**, *6*, 6687.
[136] Z. Li, Z. Hu, J. Peng, C. Wu, Y. Yang, F. Feng, P. Gao, J. Yang, Y. Xie, *Adv. Funct. Mater.* **2014**, *24*, 1821.
[137] L. F. Hu, J. Yan, M. Y. Liao, H. J. Xiang, X. G. Gong, L. D. Zhang, X. S. Fang, *Adv. Mater.* **2012**, *24*, 2305.
[138] L. F. Hu, J. Yan, Y. Kim, G. T. Fei, K. Watanabe, T. Sekiguchi, L. D. Zhang, X. S. Fang, *Small* **2015**, *11*, 1531.
[139] L. Ma, W. Hu, Q. Zhang, P. Ren, X. Zhuang, H. Zhou, J. Xu, H. Li, Z. Shan, X. Wang, *Nano Lett.* **2014**, *14*, 694.
[140] P. Guo, W. Hu, Q. Zhang, X. Zhuang, X. Zhu, H. Zhou, Z. Shan, J. Xu, A. L. Pan, *Adv. Mater.* **2014**, *26*, 2844.
[141] D. Wu, Y. Jiang, X. Yao, Y. Chang, Y. Zhang, Y. Yu, Z. Zhu, Y. Zhang, X. Lan, H. Zhong, *J. Mater. Chem. C* **2014**, *2*, 6547.
[142] W. S. Wong, S. Raychaudhuri, R. Lujan, S. Sambandan, R. A. Street, *Nano Lett.* **2011**, *11*, 2214.
[143] X. He, N. Fujimura, J. M. Lloyd, K. J. Erickson, A. A. Talin, Q. Zhang, W. Gao, Q. Jiang, Y. Kawano, R. H. Hauge, F. Leonard, J. Kono, *Nano Lett.* **2014**, *14*, 3953.
[144] D. S. Tsai, C. A. Lin, W. C. Lien, H. C. Chang, Y. L. Wang, J. H. He, *ACS Nano* **2011**, *5*, 7748.
[145] X. S. Fang, Y. Bando, M. Y. Liao, T. Y. Zhai, U. K. Gautam, L. Li, Y. Koide, D. Golberg, *Adv. Funct. Mater.* **2010**, *20*, 500.
[146] Y. Q. Liu, M. Zhang, F. X. Wang, G. B. Pan, *J. Mater. Chem. C* **2014**, *2*, 240.
[147] C. Yan, N. Singh, P. S. Lee, *Appl. Phys. Lett.* **2010**, *96*, 053108.
[148] H. Lin, H. Liu, X. Qian, S.-W. Lai, Y. Li, N. Chen, C. Ouyang, C.-M. Che, Y. Li, *Inorg. Chem.* **2011**, *50*, 7749.
[149] Q. Hong, Y. Cao, J. Xu, H. Lu, J. He, J. L. Sun, *ACS Appl. Mater. Interfaces* **2014**, *6*, 20887.
[150] J. Svensson, N. Anttu, N. Vainorius, B. M. Borg, L. E. Wernersson, *Nano Lett.* **2013**, *13*, 1380.
[151] Y. Yoon, K. Park, J. Heo, J. Park, S. Nahm, K. Choi, *J. Mater. Chem.* **2010**, *20*, 2386.
[152] Y. Xie, L. Wei, Q. Li, Y. Chen, S. Yan, J. Jiao, G. Liu, L. Mei, *Nanotechnology* **2014**, *25*, 075202.
[153] R. Zou, Z. Zhang, Q. Liu, J. Hu, L. W. Sang, M. Y. Liao, W. Zhang, *Small* **2014**, *10*, 1848.
[154] A. Zhang, H. Kim, J. Cheng, Y. H. Lo, *Nano Lett.* **2010**, *10*, 2117.
[155] J. John, M. Muthee, M. Yogeesh, S. K. Yngvesson, K. R. Carter, *Adv. Opt. Mater.* **2014**, *2*, 581.
[156] S. Komiyama, O. Astafiev, V. Antonov, T. Kutsuwa, *Microelectron. Eng.* **2002**, *63*, 173.
[157] Y. Kawano, T. Fuse, S. Toyokawa, T. Uchida, K. Ishibashi, *J. Appl. Phys.* **2008**, *103*, 034307.
[158] J. Wu, D. Shao, V. G. Dorogan, A. Z. Li, S. Li, E. A. DeCuir Jr., M. O. Manasreh, Z. M. Wang, Y. I. Mazur, G. J. Salamo, *Nano Lett.* **2010**, *10*, 1512.
[159] Y. W. Liu, D. K. Ko, S. J. Oh, T. R. Gordon, V. Doan-Nguyen, T. Paik, Y. Kang, X. Ye, L. Jin, C. R. Kagan, *Chem. Mater.* **2011**, *23*, 4657.
[160] R. Saran, M. N. Nordin, R. J. Curry, *Adv. Funct. Mater.* **2013**, *23*, 4149.
[161] M. Eita, A. Usman, A. O. El-Ballouli, E. Alarousu, O. M. Bakr, O. F. Mohammed, *Small* **2015**, *11*, 112.
[162] S. A. McDonald, G. Konstantatos, S. Zhang, P. W. Cyr, E. J. Klem, L. Levina, E. H. Sargent, *Nat. Mater.* **2005**, *4*, 138.
[163] G. Wang, X. Yang, F. Qian, J. Z. Zhang, Y. Li, *Nano Lett.* **2010**, *10*, 1088.
[164] L. J. Zhao, L. F. Hu, X. S. Fang, *Adv. Funct. Mater.* **2012**, *22*, 1551.
[165] G. Sarasqueta, K. R. Choudhury, F. So, *Chem. Mater.* **2010**, *22*, 3496.
[166] G. Sarasqueta, K. R. Choudhury, J. Subbiah, F. So, *Adv. Funct. Mater.* **2011**, *21*, 167.
[167] Q. Zhang, J. Jie, S. Diao, Z. Shao, Q. Zhang, L. Wang, W. Deng, W. Hu, H. Xia, X. Yuan, *ACS Nano* **2015**, *9*, 1561.
[168] M. Bacon, S. J. Bradley, T. Nann, *Part. Part. Syst. Charact.* **2014**, *31*, 415.
[169] J.-S. Lee, M. V. Kovalenko, J. Huang, D. S. Chung, D. V. Talapin, *Nat. Nanotechnol.* **2011**, *6*, 348.
[170] D. V. Talapin, J. S. Lee, M. V. Kovalenko, E. V. Shevchenko, *Chem. Rev.* **2009**, *110*, 389.
[171] C. O. Kim, S. W. Hwang, S. Kim, D. H. Shin, S. S. Kang, J. M. Kim, C. W. Jang, J. H. Kim, K. W. Lee, S. H. Choi, *Sci. Rep.* **2014**, *4*, 5603.
[172] Graphene Sensor is 1000 Times More Sensitive to Light, Could Enable Ultra-Low-Light Photography, http://www.extremetech.com/extreme/157082-graphene-sensor-is-1000-times-more-sensitive-to-light-could-enable-ultra-low-light-photography (accessed: September, 2015).
[173] J.-J. Wang, J.-S. Hu, Y.-G. Guo, L.-J. Wan, *NPG Asia Mater.* **2012**, *4*, e2.
[174] D. J. Xue, J. J. Wang, Y. Q. Wang, S. Xin, Y. G. Guo, L. J. Wan, *Adv. Mater.* **2011**, *23*, 3704.
[175] J.-J. Wang, Y.-Q. Wang, F.-F. Cao, Y.-G. Guo, L.-J. Wan, *J. Am. Chem. Soc.* **2010**, *132*, 12218.
[176] C. R. Dean, A. F. Young, I. Meric, C. Lee, L. Wang, S. Sorgenfrei, K. Watanabe, T. Taniguchi, P. Kim, K. L. Shepard, *Nat. Nanotechnol.* **2010**, *5*, 722.
[177] G. Konstantatos, M. Badioli, L. Gaudreau, J. Osmond, M. Bernechea, F. P. G. de Arquer, F. Gatti, F. H. Koppens, *Nat. Nanotechnol.* **2012**, *7*, 363.
[178] Z. Sun, Z. Liu, J. Li, G. A. Tai, S. P. Lau, F. Yan, *Adv. Mater.* **2012**, *24*, 5878.
[179] D. I. Son, H. Y. Yang, T. W. Kim, W. I. Park, *Appl. Phys. Lett.* **2013**, *102*, 021105.
[180] L. Leu, J. Gardner, S. Forrest, *J. Appl. Phys.* **1991**, *69*, 1052.
[181] Z. Yu, M. Aceves-Mijares, J. L. Lopez, J. Deng, *ISPDI* **2009**, 73811H.
[182] P. S. Shaw, T. C. Larason, R. Gupta, S. W. Brown, K. R. Lykke, *J. Res. Natl. Inst. Stand. Technol.* **2000**, *105*, 689.
[183] B. Levine, K. Choi, C. Bethea, J. Walker, R. Malik, *Appl. Phys. Lett.* **1987**, *50*, 1092.
[184] K. W. Liu, M. Sakurai, M. Aono, D. Shen, *Adv. Funct. Mater.* **2015**, *25*, 3157.
[185] W. Li, J. Valentine, *Nano Lett.* **2014**, *14*, 3510.
[186] M. Chen, L. Shao, S. V. Kershaw, H. Yu, J. Wang, A. L. Rogach, N. Zhao, *ACS Nano* **2014**, *8*, 8208.
[187] Y. Yao, R. Shankar, P. Rauter, Y. Song, J. Kong, M. Loncar, F. Capasso, *Nano Lett.* **2014**, *14*, 3749.

[188] P. Senanayake, C. H. Hung, J. Shapiro, A. Lin, B. Liang, B. S. Williams, D. Huffaker, *Nano Lett.* **2011**, *11*, 5279.
[189] T. Echtermeyer, L. Britnell, P. Jasnos, A. Lombardo, R. Gorbachev, A. Grigorenko, A. Geim, A. Ferrari, K. Novoselov, *Nat. Commun.* **2011**, *2*, 458.
[190] V. Popov, D. Fateev, T. Otsuji, Y. Meziani, D. Coquillat, W. Knap, *Appl. Phys. Lett.* **2011**, *99*, 243504.
[191] P. Berini, *Laser Photonics Rev.* **2014**, *8*, 197.
[192] C. C. Chang, Y. D. Sharma, Y. S. Kim, J. A. Bur, R. V. Shenoi, S. Krishna, D. Huang, S. Y. Lin, *Nano Lett.* **2010**, *10*, 1704.
[193] H. Chalabi, D. Schoen, M. L. Brongersma, *Nano Lett.* **2014**, *14*, 1374.
[194] A. Sobhani, M. W. Knight, Y. Wang, B. Zheng, N. S. King, L. V. Brown, Z. Fang, P. Nordlander, N. J. Halas, *Nat. Commun.* **2013**, *4*, 1643.
[195] Z. Fang, Z. Liu, Y. Wang, P. M. Ajayan, P. Nordlander, N. J. Halas, *Nano Lett.* **2012**, *12*, 3808.
[196] Y. Liu, R. Cheng, L. Liao, H. Zhou, J. Bai, G. Liu, L. Liu, Y. Huang, X. F. Duan, *Nat. Commun.* **2011**, *2*, 579.
[197] V. J. Sorger, R. F. Oulton, R. M. Ma, X. Zhang, *MRS Bull.* **2012**, *37*, 728.
[198] Z. L. Wang, *Adv. Mater.* **2012**, *24*, 4632.
[199] Z. L. Wang, *Nano Today* **2010**, *5*, 540.
[200] Z. Wang, R. Yu, C. Pan, Y. Liu, Y. Ding, Z. L. Wang, *Adv. Mater.* **2015**, *27*, 1553.
[201] N. Bristowe, T. Fix, M. Blamire, P. Littlewood, E. Artacho, *Phys. Rev. Lett.* **2012**, *108*, 166802.
[202] H. L. Lu, Z. M. Liao, L. Zhang, W. T. Yuan, Y. Wang, X. M. Ma, D. P. Yu, *Sci. Rep.* **2013**, *3*, 2870.
[203] N. C. Bristowe, G. Philippe, P. B. Littlewood, A. Emilio, *J. Phys.: Condens. Matter* **2014**, *26*, 143201.
[204] H. Li, J. Yang, J. Zhang, M. Zhou, *RSC Adv.* **2012**, *2*, 6258.
[205] F. H. Teherani, D. C. Look, D. J. Rogers, T. Pauporté, O. Lupan, B. Viana, L. Chow, M. Tchernycheva, *Proc. SPIE 8987*, SPIE, San Francisco, CA, USA, **2014**, 89871R.
[206] X. Wang, Z. Xie, H. Huang, Z. Liu, D. Chen, G. Z. Shen, *J. Mater. Chem.* **2012**, *22*, 6845.
[207] J. G. Lu, P. Chang, Z. Y. Fan, *Mater. Sci. Eng. R: Rep.* **2006**, *52*, 49.
[208] X. Wang, Y. Zhang, X. Chen, M. He, C. Liu, Y. Yin, X. Zou, S. Li, *Nanoscale* **2014**, *6*, 12009.
[209] S. J. Choi, Y. C. Lee, M. L. Seol, J. H. Ahn, S. Kim, D. I. Moon, J. W. Han, S. Mann, J. W. Yang, Y. K. Choi, *Adv. Mater.* **2011**, *23*, 3979.
[210] W. I. Park, J. S. Kim, G. C. Yi, H. J. Lee, *Adv. Mater.* **2005**, *17*, 1393.
[211] N. Liu, G. Fang, W. Zeng, H. Zhou, H. Long, X. Zou, Y. Liu, X. Zhao, *Appl. Phys. Lett.* **2010**, *97*, 243504.
[212] R. M. Ma, L. Dai, H. B. Huo, W. J. Xu, G. Qin, *Nano Lett.* **2007**, *7*, 3300.
[213] P. Wu, Y. Ye, T. Sun, R. Peng, X. Wen, W. Xu, C. Liu, L. Dai, *ACS Nano* **2009**, *3*, 3138.
[214] M. Mongillo, P. Spathis, G. Katsaros, P. Gentile, S. De Franceschi, *Nano Lett.* **2012**, *12*, 3074.
[215] H. Wang, L. Yu, Y. H. Lee, Y. Shi, A. Hsu, M. L. Chin, L. J. Li, M. Dubey, J. Kong, T. Palacios, *Nano Lett.* **2012**, *12*, 4674.
[216] W. Zheng, F. Huang, R. Zheng, H. Wu, *Adv Mater.* **2015**, *27*, 3921.
[217] C. Xie, B. Nie, L. Zeng, F. X. Liang, M. Z. Wang, L. Luo, M. Feng, Y. Yu, C. Y. Wu, Y. Wu, *ACS Nano* **2014**, *8*, 4015.
[218] G. H. Chen, Y. Q. Yu, K. Zheng, T. Ding, W. L. Wang, Y. Jiang, Q. Yang, *Small* **2015**, *11*, 2848.
[219] L. Vicarelli, M. Vitiello, D. Coquillat, A. Lombardo, A. Ferrari, W. Knap, M. Polini, V. Pellegrini, A. Tredicucci, *Nat. Mater.* **2012**, *11*, 865.